

Anticancer and antimicrobial activities of a novel 4-nitrobenzohydrazone and the Cu(II), Ni(II), Co(II), and Mn(II) complexes

Chigozie J. O. Anarado, Ebuka H. Onyilogwu, Chigozie J. Ezeorah, Nnaemeka Nnaji, Chukwujindu M. A. Iwegbue, Ilknur Babahan-Bircan, Fatih Eyduan, Esin Poyrazoglu Coban, Muruvvet Abbak, Ali Özmen, Safiye Emirdağ Öztürk, Ilke Demirkaya, Halil Biyik & Oguejiofo T. Ujam

To cite this article: Chigozie J. O. Anarado, Ebuka H. Onyilogwu, Chigozie J. Ezeorah, Nnaemeka Nnaji, Chukwujindu M. A. Iwegbue, Ilknur Babahan-Bircan, Fatih Eyduan, Esin Poyrazoglu Coban, Muruvvet Abbak, Ali Özmen, Safiye Emirdağ Öztürk, Ilke Demirkaya, Halil Biyik & Oguejiofo T. Ujam (2023): Anticancer and antimicrobial activities of a novel 4-nitrobenzohydrazone and the Cu(II), Ni(II), Co(II), and Mn(II) complexes, *Inorganic and Nano-Metal Chemistry*, DOI: [10.1080/24701556.2023.2235328](https://doi.org/10.1080/24701556.2023.2235328)

To link to this article: <https://doi.org/10.1080/24701556.2023.2235328>



View supplementary material [↗](#)



Published online: 23 Jul 2023.



Submit your article to this journal [↗](#)




View related articles [↗](#)



View Crossmark data [↗](#)



Anticancer and antimicrobial activities of a novel 4-nitrobenzohydrazone and the Cu(II), Ni(II), Co(II), and Mn(II) complexes

Chigozie J. O. Anarado^a, Ebuka H. Onyilogwu^a, Chigozie J. Ezeorah^b, Nnaemeka Nnaji^c, Chukwujindu M. A. Iwegbue^d, Ilknur Babahan-Bircan^e, Fatih Eydurhan^e, Esin Poyrazoglu Coban^f, Muruvvet Abbak^g, Ali Özmen^f, Safiye Emirdağ Öztürk^h, Ilke Demirkaya^e, Halil Biyik^f, and Oguejiofo T. Ujam^b 

^aDepartment of Pure and Industrial Chemistry, Nnamdi Azikiwe University, Awka, Anambra State, Nigeria; ^bDepartment of Pure and Industrial Chemistry, University of Nigeria, Nsukka, Enugu State, Nigeria; ^cDepartment of Chemistry, Faculty of Physical Sciences, Alex Ekwueme Federal University Ndufu Alike Ikwo, Abakaliki, Ebonyi State, Nigeria; ^dDepartment of Chemistry, Delta State University, Abraka, Nigeria; ^eDepartment of Chemistry, Faculty of Arts and Sciences, Aydin Adnan Menderes University, Aydin, Turkey; ^fDepartment of Biophysics, Faculty of Medicine, Aydin Adnan Menderes University, Aydin, Turkey; ^gScience Technology Research and Application Centre, Aydin Adnan Menderes University, Aydin, Turkey; ^hDepartment of Chemistry, Faculty of Arts and Sciences, Ege University, Izmir, Turkey

ABSTRACT

Antimicrobial and anticancer activities against prostate (PC-3) and breast (MCF-7) cancer cells by Schiff base derived from novel 4-Nitrobenzohydrazone ligand and its Cu(II), Ni(II), Co(II), and Mn(II) complexes are reported in this study. Characterizations by conventional spectroscopic techniques and elemental analyses suggest successful syntheses. The cobalt complex, Co(HL)₂ was found to be moderately effective on both *Pseudomonas aeruginosa* ATCC 35032 and *Candida albicans* ATCC 10231, other compounds did not affect the test microorganisms. Results indicated that the compounds are effective on both prostate and breast cell lines at concentrations between 5 and 40 μ M, and exhibit their effects by apoptotic mechanisms. The complex Mn(HL)₂ could be a potential candidate against prostate cancer cells (PC-3). The interactions of ligand and complexes with biological targets were predicted by molecular docking which indicated high binding affinities, and artificial neural network explained their anticancer activities. Density functional theoretical calculations corroborated experimental findings.

ARTICLE HISTORY

Received 9 September 2022
Accepted 5 July 2023

KEYWORDS



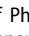
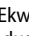
4-nitrobenzohydrazone;
metal complexes;
antimicrobial; prostate
cancer (PC-3); breast cancer
(MCF-7)


1. Introduction

Hydrazones and their metal complexes have been molecules of research interest toward the discovery of biological friendly anti-pathogenic agents. Reportedly, they exhibit biological activities viz. antiviral, antibacterial, anticonvulsant, anti-inflammatory, antimalarial, analgesic, and antipyretic properties.^[1–5] These activities have been mainly attributed to the biological adaptability or reactivity of the azomethine moiety (–NHN=CH–) in hydrazones.^[6] Apart from their rich biological activities, their facile synthetic routes through a condensation reaction of ketones or aldehydes with hydrazides, make them easily accessible. An advantage that helps in fine-tuning the molecular properties for targeted application. Hydrazones of dehydroacetic acid and the metal complexes show good biological activities against pathogens.^[7] Reportedly, hydrazones are known to have good ligating abilities toward transition metal ions resulting in the formation of complexes with interesting structures.^[8–12] Hydrazones and their metal complexes have also been found to interact/bind with DNA either causing its damage or

inhibiting its replication.^[13] Their cytotoxicity assays on cancer cells have had physiological effects on rapidly dividing cancer cell lines. This potential makes them invaluable agents in the chemotherapeutic treatment of cancer. They can bind with the DNA in quite many modes. The most important binding mode is intercalation because it leads to cell destruction.^[14] This is a non-covalent binding mode that involves the fitting-in of these compounds between the genomic structures.^[15,16] Since the DNA binding activity of a drug helps in determining its efficacy, intercalation as a binding mode has been quite helpful in probing the biological actions of drugs.^[17,18]

Despite the availability of a large number of antiproliferative and antimicrobial agents, there has been a search for novel and more efficient antiproliferative and antimicrobial agents with less bio-toxicity. The more challenging aspect of microbial evolution is the emergence of multidrug-resistant strains which pose a serious threat to human life and health management systems globally. These strains mutate and thus, resist conventional drugs.^[19] To date, drug design stands as the only headway toward solving these global

CONTACT Nnaemeka Nnaji  joemek4u@yahoo.com  Department of Chemistry, Faculty of Physical Sciences, Alex Ekwueme Federal University Ndufu Alike Ikwo, Abakaliki, Ebonyi State, Nigeria; Oguejiofo T. Ujam  oguejiofo.ujam@unn.edu.ng  Department of Pure and Industrial Chemistry, University of Nigeria, Nsukka 410001, Enugu State, Nigeria.

 Supplemental data for this article can be accessed online at <https://doi.org/10.1080/24701556.2023.2235328>.

© 2023 Taylor & Francis Group, LLC

health issues. The design could involve changing the organic scaffold and/or the metal ion to obtain novel molecules with a novel mechanism of action.

The uv-vis absorption properties of aromatic compounds containing hetro atoms and π -electron conjugation affect their electron donating and withdrawing strengths. This is also influenced by solvent(s) and this agrees with earlier literature report.^[20] Time-dependent density functional theory (TD-DFT) is effective for prediction/estimation of uv-vis absorption of compounds.^[20] The effectiveness of TD-DFT in describing uv-vis spectra of compounds necessitated its use to enhance understanding of the absorption spectra of Schiff bases, anthraquinones, neoflavonoids and flavonoids.^[20,21] Herein, we report the studies of uv-vis spectra of the Schiff base in different solvents.^[20–24]

The application of computer-aided techniques in discovery of antibiotics is vital because they are faster and comparatively cheaper than the more expensive and labor intensive traditional high-throughput screens and lead-optimization efforts.^[22] Herein therefore, this work applied the principal component analysis and density functional techniques to validate the antibiotic and anticancer properties of the compounds.

To the best of our knowledge there is no report of the antimicrobial activity and anti-cancer investigations against prostate and breast cancer cells of the new compounds in literature. To add to the bank of other available knowledge in literature, we report in the present contribution the synthesis and spectroscopic characterization of a novel hydrazide hydrazone ligand 2-hydroxy-6-methyl-4-oxo-4H-pyran-3-yl)ethylidene-4-nitrobenzohydrazide and its Cu(II), Ni(II), Co(II), and Mn(II) complexes.

2. Experimental

2.1. Materials

Analytical grade starting chemicals, 4-nitrobenzohydrazide and sodium bicarbonate (Sigma–Aldrich). Dehydroacetic acid (Merck, Germany). The nickel(II) chloride hexahydrate and manganese(II) chloride tetrahydrate (Guangdong Guanghua Sci-Tech Co. Ltd), copper(II) chloride dihydrate {Sure Chem. Products (SCP Ltd. England)}, cobalt(II) chloride hexahydrate {Cartivalue Chemicals (Cartivalue Chemicals Ltd., Mumbai, India)} and solvents MeOH (SigmaAldrich) were used as supplied.

2.2. Physical methods

The ^1H and ^{13}C NMR spectra of the ligand and the complexes were recorded on Bruker at 400 MHz in DMSO- d_6 solvent. Infrared (IR) spectral data for all the compounds were recorded on Varian in the 4000–400 cm^{-1} range using KBr disk. The micro elemental analysis C, H, N of the compounds was carried out with Leco/Truespec Micro. The electronic spectra were recorded using Pye-Unicam in DMSO as a solvent. The Electrospray Ionization Mass Spectra (ESI-MS) for the compounds were obtained with a Thermo TSQ

in positive ion mode using pneumatically assisted electrospray ionization: capillary of voltage, 2900 V; sample cone voltage, 15 V; extraction voltage, 1 V; source temperature, 80 °C; desolvation temperature, 160 °C; cone gas flow, 100 Lh^{-1} ; desolvation gas flow, 100 Lh^{-1} ; collision voltage, 2 V; MCP voltage, 2400 V. No smoothening of the data was performed, and a comparison of observed and calculated isotope patterns was used in the ion assignment.^[25,26]

2.3. Synthesis

2.3.1. Synthesis of 2-hydroxy-6-methyl-4-oxo-4H-pyran-3-yl)ethylidene-4-nitrobenzohydrazide (HL)

Dehydroacetic acid (2270 mg, 13.50 mmol) was dissolved in 40 mL methanol and heated for three minutes while stirring on a magnetic stirrer hot plate. 4-nitrobenzohydrazide (2450 mg, 13.50 mmol) was added, followed by sodium bicarbonate (1130 mg, 13.50 mmol) and the mixture was refluxed for 1 h. The resulting orange precipitate was allowed to cool, filtered and washed with methanol ($3 \times 10\text{ mL}$). The precipitated products were obtained by slow evaporation of the filtrate and washed with methanol (20 mL), and dried at room temperature.

Yield: 82%; m.p: 270 °C; Color: orange; Selected IR data (KBr, ν/cm^{-1}): 3435b $\nu(\text{O-H str})$, 2848 m, 2919 m $\nu(\text{aliphatic C-H str})$, 1636.91 s $\nu(\text{C=O str})$, 1501 m $\nu(\text{C=N})$, 1356 m, 1460 m $\nu(\text{N-O str})$, 1189 m, 1275 m $\nu(\text{C-O str})$, 749 s $\nu(\text{wagging N-H})$. ^1H NMR (400 MHz, DMSO- d_6 , ppm): 15.61 (s, 1H, OH), 10.12 (s, 1H, -NH), 8.28–8.15 (m, 4H, ArH nitrobenzene), 8.03 (s, 1H, ArH pyrone), 2.89 (s, 3H, CH_3 pyrone), 2.73 (s, 3H, $\text{CH}_3\text{-C=N-}$). ^{13}C NMR (400 MHz, DMSO- d_6 , ppm): 181.23 (C, C=O pyrone), 164.34, 164.20, 164.12 (C, -NH-C=O), 160.14 (C, C-OH), 157.60 (C, -C=N-), 147.96–124.00 (C atoms, nitrobenzene), 19.54, 19.52 (C, CH_3 pyrone), 17.28 (C, CH_3 attached to azomethine). ESI-MS (m/z): (331.11 $[\text{M}]^+$, 33%, 349.25 $[\text{M} + \text{NH}_4]^+$, 57%, 371.09 $[\text{M} + \text{ONa}]^+$, 28%), Cal. = 331.28. Anal. Calc. for $\text{C}_{15}\text{H}_{13}\text{O}_6\text{N}_3$ (331.28): C, 54.38; H, 3.93; N, 12.69. Found: C, 53.08; H, 3.97; N, 11.29%. UV-visible (λ_{max} , DMSO, nm): 226.5 ($\pi \rightarrow \pi^*$), 276.5, 361 ($n \rightarrow \pi^*$).

2.4. Synthesis of metal(II) 2-hydroxy-6-methyl-4-oxo-4H-pyran-3-yl)ethylidene-4-nitrobenzohydrazide

2.4.1. Cu(HL) synthesis

The ligand, HL (450 mg, 1.36 mmol) was dissolved in methanol (20 mL) and heated for two minutes while stirring on a magnetic stirrer hot plate. Copper(II) chloride dihydrate (230 mg, 1.36 mmol) was added gradually to the stirred solution of the ligand and the mixture was refluxed for 2 h. The resulting acid green precipitates was allowed to cool, filtered and washed with methanol ($3 \times 10\text{ mL}$). The product was allowed to dry at room temperature.

Yield: 75%; m.p: 254 °C; Color: acid green; Selected IR data (KBr, ν/cm^{-1}): 3446b $\nu(\text{O-H str})$, 2848 m, 2915 m, $\nu(\text{aliphatic C-H str})$, 1636.30 s $\nu(\text{C=O str})$, 1484 m $\nu(\text{C=N})$, 749 s $\nu(\text{wagging N-H})$, 711 m $\nu(\text{M-Cl str})$, 668 m $\nu(\text{M-N str})$, 416 m $\nu(\text{M-O str})$. ESI-MS (m/z): (445.17 $[\text{M}]^+$,

85%), Cal. = 446.94. Anal. Calc. for $C_{15}H_{15}O_7N_3ClCu$ (446.94): C, 40.27; H, 3.13; N, 9.40. Found: C, 39.04; H, 2.83; N, 8.13%. UV-visible (λ_{max} , DMSO, nm): 408 ($d-d$ transition).

2.4.2. Ni(HL)₂ synthesis

The ligand, HL (450 mg, 1.36 mmol) was dissolved in methanol (20 mL) and heated for two minutes while stirring on a magnetic stirrer hot plate. Nickel(II) chloride hexahydrate (160 mg, 0.68 mmol) was added gradually to the stirred solution of the ligand and the mixture was refluxed for 2 h. The resulting golden precipitate was allowed to cool, filtered and washed with methanol (3×10 mL). The residue was allowed to dry at room temperature.

Yield: 82%; m.p: 285 °C; Color: gold; Selected IR data (KBr, ν/cm^{-1}): 3434b $\nu(O-H$ str), 2848 m, 2919 m, ν (aliphatic C-H str), 1626.40 s $\nu(C=O$ str), 1565 m $\nu(C=N)$, 749 s ν (wagging N-H), 545 m $\nu(M-N$ str), 437 m $\nu(M-O$ str). ESI-MS (m/z): (721.59 $[M+H]^+$, 66%), Cal. = 720.69. Anal. Calc. for $C_{30}H_{26}O_{12}N_6Ni$ (720.69): C, 49.95; H, 3.61; N, 11.66. Found: C, 48.03; H, 2.94; N, 10.03%. UV-visible (λ_{max} , DMSO, nm): 274.5 ($\pi \rightarrow \pi^*$), 349.5 ($n \rightarrow \pi^*$), 433 ($^3A_{2g}(F) \rightarrow ^3T_{1g}(F)$ transition).

2.4.3. Co(HL)₂ synthesis

Ligand, HL (450 mg, 1.36 mmol) was dissolved in methanol (20 mL) and heated for two minutes while stirring on a magnetic stirrer hot plate. Cobalt(II) chloride hexahydrate (160 mg, 0.68 mmol) was added gradually to the stirred solution of the ligand and the mixture was refluxed for 2 h. The resulting dark orange precipitate was allowed to cool, filtered and washed with methanol (3×10 mL). The product was allowed to dry at room temperature.

Yield: 65%; m.p: 265 °C; Color: dark orange; Selected IR data (KBr, ν/cm^{-1}): 3390b $\nu(O-H$ str), 2848 m, 2915 m, ν (aliphatic C-H str), 1692.06 s, 1630.44 $\nu(C=O$ str), 1595s $\nu(C=N)$, 749 s ν (wagging N-H), 607 m $\nu(M-N$ str), 443 m $\nu(M-O$ str). ESI-MS (m/z): (744.97 $[M+Na]^+$, 33%), Cal. = 721. Anal. Calc. for $C_{30}H_{26}O_{12}N_6Co$ (721): C, 49.93; H, 3.61; N, 11.65. Found: 49.63; H, 3.15; N, 11.64%. UV-visible (λ_{max} , DMSO, nm): 240, 268.5 ($\pi \rightarrow \pi^*$), 356.5 ($n \rightarrow \pi^*$), 425 ($^4T_{1g}(F) \rightarrow ^4A_{2g}(F)$ transition).

2.4.4. Mn(HL)₂

Ligand, HL (450 mg, 1.36 mmol) was dissolved in methanol (20 mL) and heated for two minutes while stirring on a magnetic stirrer hot plate. Manganese(II) chloride tetrahydrate (130 mg, 0.68 mmol) was added gradually to the stirred solution of the ligand and the mixture was refluxed for 2 h. The resulting brown precipitate was allowed to cool, filtered and washed with methanol (3×10 mL). The product was allowed to dry at room temperature.

Yield: 88%; m.p: 263 °C; Color: brown; Selected IR data (KBr, ν/cm^{-1}): 3444b $\nu(O-H$ str), 2848 m, 2916 m, ν (aliphatic C-H str), 1634.86 s $\nu(C=O$ str), 1547 m $\nu(C=N)$, 749 s ν (wagging N-H), 587 m $\nu(M-N$ str), 420 m $\nu(M-O$

str). ESI-MS (m/z): (717.48 $[M+H]^+$, 36%), Cal. = 716.93. Anal. Calc. for $C_{30}H_{26}O_{12}N_6Mn$ (716.93): C, 50.21; H, 3.63; N, 11.72. Found: C, 49.99; H, 3.95; N, 10.32%. UV-visible (λ_{max} , DMSO, nm): 210 ($\pi \rightarrow \pi^*$), 270.5 ($n \rightarrow \pi^*$), 426.5 ($^6A_{1g}(S) \rightarrow ^2A_{1g}(I)$ transition).

2.5. Antimicrobial screening

2.5.1. Microorganisms and condition for cultivation

The seventeen bacteria, eleven yeasts, and four microfungi were used to test the antimicrobial effect. The Gram-negative (G-) strains were *Escherichia coli* ATCC 35218, *Enterobacter aerogenes* ATCC 13048, *Salmonella typhimurium* ATCC 14028, *Klebsiella pneumoniae* ATCC 13882, *Pseudomonas aeruginosa* ATCC 35032, *Serratia marcescens* ATCC 13880, *Proteus vulgaris* ATCC 33420. The Gram-positive (G+) strains were *Micrococcus luteus* ATCC 9341, *Staphylococcus aureus* ATCC 25923, *Staphylococcus epidermidis* ATCC 12228, *Streptococcus pneumoniae* ATCC 27336, *Corynebacterium xerosis* ATCC 373, *Mycobacterium smegmatis* ATCC 607, *Enterococcus faecalis* ATCC 29212, *Listeria monocytogenes* ATCC 19112, *Bacillus cereus* ATCC 11778, *Bacillus subtilis* ATCC 6633. The yeast strains were *Candida albicans* ATCC 10231, *Candida utilis* ATCC 9950, *Candida tropicalis*, *Candida glabrata*, *Saccharomyces cerevisiae* ATCC 9763, *Debaryomyces hansenii* NRRL Y-1458, *Torulaspora delbrueckii*, *Hansenula philodendron*, *Pichia pastoris*, *Kluyveromyces fragilis*, *Dekkera bruxellensis*, *Aspergillus niger*, *Aspergillus flavus*, *Aspergillus fumigatus*, *Aspergillus foetidus*. The twenty strains were obtained from the American Type Culture Collection (ATCC, Rockville, MD, USA) and one yeast strain was provided from the Agricultural Research Service Culture Collection (ARS, NRRL, Peoria, USA). Other strains were obtained from the Department of Microbiology, Faculty of Sciences, Ege, and Adnan Menderes University. The bacterial strains were cultured in Tryptic Soy Agar (TSA) and Brain Heart Infusion Agar (BHIA) at 30–37 °C for 24 h. The yeast strains were cultured in Malt Extract Agar (MEA) at 30 °C for 24 h.^[27] The microfungi strains were cultured in Potato Dextrose Agar (PDA) at 25–27 °C for 5–7 days.^[27,28]

2.5.2. Antimicrobial assays

The antimicrobial activities of the compounds were determined by the agar well diffusion method.^[29–31] The minimum inhibitory concentrations (MIC) were obtained by broth dilution method.^[32–34]

2.5.3. Disk diffusion method

Screening for antimicrobial activities was carried out by the agar well diffusion method against test microorganisms.^[29–31] The inoculum suspensions of the tested bacteria and yeasts were prepared from the broth cultures (18–24 h) and the turbidity equivalent was adjusted to 0.5 McFarland standard tube to give a concentration of 1×10^8 bacterial cells/mL, 1×10^6 yeast cells/mL.^[28,35–37] The microfungi suspensions were adjusted as 1×10^4 conidia cells/mL.^[27] To test the

antimicrobial activity of the compounds, 20 ml of Mueller Hinton Agar (MHA) were poured into Petri dishes and kept to solidify at room temperature. Then, it was inoculated with strains of bacteria, yeasts, and fungi by taking 0.1 ml from cell culture media. Then, a hole of 6 mm in diameter and depth were made on top with a sterile stick and was filled with 50 μ l of compounds solution. Then, bacterial cultures were incubated at 30–37 °C, yeast cultures were incubated at 27–30 °C for 18–24 h. The fungi cultures were incubated at 25–27 °C for 5–7 days. At the end of incubation time, the diameters of the inhibition zones formed on the MHA were evaluated in millimeters. Disks containing Chloramphenicol (30 mg Oxoid), Gentamycin (10 mg Oxoid), Tetracycline (30 mg Oxoid), Erythromycin (15 mg Oxoid), Penicilin (10 mg Oxoid), Ampicillin (10 mg Oxoid), Vancomycin (30 mg Oxoid), Ofloxacin (5 mg Oxoid) for bacteria, and Nystatin (100 mg Oxoid) for yeasts, and Clotrimazole (10 mg Oxoid) for microfungi were used as positive controls. The measured inhibition zones of the study compounds were compared with those of the reference disks^[27,28,38]

2.5.4. Dilution method

The antibacterial and antifungal activities of synthesized compounds were examined by preparing a microdilution broth.^[32–34] The analysis was carried out in a sterile 96-well microtitre plate. The suspensions adjusted as 1×10^8 bacterial cells/mL, 1×10^6 yeast cells/mL, and 1×10^4 conidia cells/mL for the analysis were used. Initially, 100 μ L of Mueller Hinton Broth (MHB) was placed in each well. After, the compounds were added to the first well. Two-fold serial dilutions of the compounds were carried out to determine the MIC, within the concentration range 256 to 0.25 μ gml⁻¹. Next, 100 μ L of microorganism suspension was added to each well. The bacterial cultures were incubated at 30–37 °C, yeast cultures were incubated at 27–30 °C for 18–24 h. The fungi cultures were incubated at 25–27 °C for 5–7 days. The lowest concentration of the study compounds that resulted in complete inhibition of the microorganisms was represented as MIC (gmL⁻¹). The lowest concentration of antimicrobial agents that resulted in complete inhibition of the microorganisms was represented as MIC (μ gmL⁻¹). The streptomycin for bacteria and fluconazole for yeasts and microfungi were used as positive controls in the dilution method.

2.6. Anti-proliferative studies

2.6.1. Cell culture

Two lines of human cancer cells were used in these experiments. Human prostate cancer PC3 cells and human breast cancer MCF7 cells were grown in RPMI-1640 and DMEM, respectively, supplemented with 10% FBS, 1% L-glutamine, and 100 U/ml penicillin and streptomycin (Sigma). Cells were maintained in a humidified atmosphere with 5% CO₂ air at 37 °C and the cells were seeded on 48 or 96 well plates with 10⁵ cell density and apoptosis measurement was maintained in 24 wells that were carried out at a cell density of

10⁶ cells ml. Cells were incubated overnight. Cells in the exponential phase of growth were used in each experiment. The cells were seeded into 48 or 96 well plates with 10⁵ cell density and apoptosis measurement was maintained in 24 wells that were carried out at a cell density of 10⁶ cells ml. After 24 h, different concentrations of drugs (5, 10, 20, 40 μ M) and 1 μ M paclitaxel (Pax) were added to the well plates, and measurements were performed on the cells.^[39,40]

2.6.2. Cell survival assay

The toxicity of products was evaluated by using 3-(4,5-Dimethylthiazol-2-yl)-2,5-diphenyltetrazolium bromide tetrazolium (MTT) reduction assay on both cancer cells. For this, 5 mg/mL MTT dye was solved in PBS and added 40 μ l to each well. After 4 h incubation, formazan crystals were dissolved by DMSO and measured 540 nm and 620 nm spectrophotometrically.^[39,40]

2.6.3. HOPI staining

Apoptosis was assessed by Hoechst and propidium iodide (HOPI) staining. The cells were seeded in a 24-well plate at a density of 10⁶ cells/well. 24 h after treatments, cells were washed with PBS, trypsinized, and centrifuged. Pellets were suspended in 50 μ L fresh medium with the addition of 0.25 μ L of Hoechst and 0.25 μ L of propidium iodide and incubated for 30 min at 37 °C in the dark. The cells were immediately analyzed by fluorescence microscopy and images were taken by Zeiss axiocam ICc5 camera.^[35,40]

2.6.4. Theoretical studies

2.6.4.1 Quantum chemical calculations. The geometry optimization of HL was performed using Becke 3-parameter Lee–Yang–Parr (B3LYP) type of a density functional theoretical (DFT) technique, using 6–31G (D) basis set.^[22,23] The geometry optimizations of complexes (CuHL, Co(HL)₂, Mn(HL)₂ and Ni(HL)₂) were done using B3LYP in conjunction with SDD basis sets.^[20] Gaussian 09 program was used to perform all calculations.^[41] The structures of the ligands and complexes were optimized in the gas phase and for calculation in methanol solvent the polarized continuum model (PCM) was used. The infrared spectra of the optimized structures of ligand and Mn(HL)₂ complex were calculated in the gas phase using the same functional and basis set. TD-DFT calculations were performed with the same functional, basis set and solvation model. The effects of methanol solvent were simulated using the polarized continuum model (PCM) considering two approaches: one technique did not consider hydrogen bonded methanol molecules, and the second approach involved hydrogen bonded methanol molecules. The consideration however is such that number of included methanol molecules depends on possible hydrogen bonding sites available in the ligand molecule.

2.6.4.2. Molecular docking. Compound structures were drawn in Arguslab 4.0 (for Windows) and optimized using the DFT technique earlier described. The optimized

structures were read as input for AutoDock 4.2 so as to carry out the docking simulations described earlier.^[21]

2.6.5. Statistical analyses

Statistical analysis was determined by using GraphPad. Cytotoxicity values were expressed as means \pm SD of at least four independent experiments, the differences among the groups were analyzed by one-way analysis of variance (one-way ANOVA), and HOPI data were analyzed by two-way analysis of variance (two-way ANOVA), $p < 0.01$, and $p < 0.05$ were considered to be significant. Artificial neural network was done using Statistical package for the Social Sciences 20.

3. Results and discussion

3.1. General synthesis

The hydrazone ligand was formed from the reaction of dehydroacetic acid and 4-nitrobenzohydrazide in methanolic solution in the presence of sodium bicarbonate to catalyze the condensation reaction which involves an electrophilic attack and elimination of water molecule (Scheme 1). Its Cu(II), Ni(II), Co(II), and Mn(II) complexes were formed by reacting the ligand with copper(II) chloride dihydrate, nickel(II) chloride hexahydrate, cobalt(II) chloride hexahydrate, and manganese(II) chloride tetrahydrate, respectively. Characterization of all the compounds was done using elemental analysis, and spectroscopic methods (ESI-MS, IR, ^1H and ^{13}C NMR, and UV-vis spectroscopies).

3.2. ^1H and ^{13}C -NMR spectra of the ligand (HL)

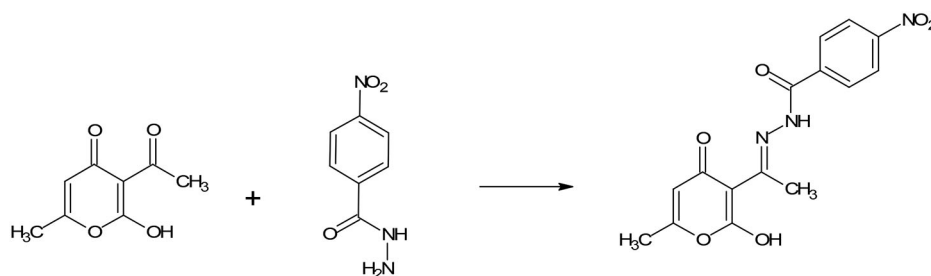
The ^1H and ^{13}C NMR spectra of the ligand are presented as supplementary materials (SM 1a,b). The ^1H NMR spectrum of the ligand gave a single peak at 15.61 ppm which is attributed to the proton of the hydroxyl group. This peak was also present in the spectra of its complexes which shows that deprotonation did not occur thus, the hydroxyl oxygen did not participate in the coordination in all the complexes. The proton of the secondary amine group gave a single peak at 10.12 ppm which was found also in the spectra of the complexes, indicating the nonparticipation of the nitrogen atom of the amine group in the coordination. The multiplet peak in the range, 8.28–8.15 ppm is attributed to the aromatic protons of the nitrobenzene ring. The aromatic proton of the pyrone ring gave a single peak at 8.03 ppm. The

protons of the methyl group attached to the pyrone ring gave a singlet at 2.89 ppm whereas the singlet at 2.73 ppm was given by the protons of the methyl group attached to the azomethine.

Using the ^{13}C -NMR spectrum of the ligand, the assignment of peaks drawn from the ^1H - NMR spectrum was authenticated. The carbon atom of the carbonyl group attached to the pyrone ring gave signal at 181.23 ppm whereas the signal at 164.34, 164.20, 164.12 ppm was given by the carbon atom of the carbonyl group attached to the secondary amine. The signal due to the carbon atom of the C-OH group was found at 160.14 ppm. The carbon atom of the azomethine group gave a peak at 157.60 ppm which shows that the ligand formed.^[42,43] The carbon atoms of the nitrobenzene ring which are in four different carbon environments, gave peaks in the range, 147.96–124.00 ppm (147.96, 145.91, 128.89/128.78, and 124.00 ppm). The peak at 19.54, 19.52 ppm was assigned to the carbon atom of the methyl group attached to the pyrone ring whereas the peak at 17.28 ppm was given by the carbon atom of the methyl group attached to the azomethine.

3.3. Mass spectra and elemental analysis

The supplementary materials (SM 2a–d) contain the mass spectra of the ligand and the complexes. The ESI-MS molecular ion signals of the ligand and its complexes were in concordance with their proposed structures. HL ligand gave molecular ion signals at $331.11 = [\text{M}]^+$, $371.09 = [\text{M} + \text{ONa}]^+$ and $349.25 = [\text{M} + \text{NH}_4]^+$ which agree with a calculated value of 331.28. The Cu(II), Ni(II), Co(II), and Mn(II) complexes of the ligand gave molecular ion peaks at $445.17 [\text{M}]^+$, $721.59 [\text{M} + \text{H}]^+$, $744.97 [\text{M} + \text{Na}]^+$, and $717.48 [\text{M} + \text{H}]^+$, respectively, which are in concordance with their calculated molecular masses of 446.94, 720.69, 721.00, and 716.93, respectively, thus, indicative of ligand to metal coordination of 2:1 for the Ni(II), Co(II), and Mn(II) complexes, and 1:1 for the Cu(II) complex. The Cu(II) complex gave a peak at m/z 410.94 which is due to the loss of the coordinated chlorine atom. Also found in the Cu(II) complex spectrum, is a m/z signal at 429.28 which is a result of the loss of the coordinated water molecule. Some unidentified m/z peaks may be due to minor adducts in the fragmentation. The elemental analyses of the ligand and its complexes gave results that are not so much in agreement with their calculated elemental compositions which could be attributed to the impure nature of the compounds.



Scheme 1. Synthesis of 2-hydroxy-6-methyl-4-oxo-4H-pyran-3-yl)ethylidene-4-nitrobenzohydrazide (HL).

3.4. Infrared spectra of the ligand (HL) and metal complexes

The Fourier-Transform Infrared Spectroscopy (FTIR) spectra of the ligand and its complexes are a good source of information on whether; there is ligand formation and its coordination with metal ions (see SM 3).

The IR spectrum of the ligand gave a broad peak at 3435 cm^{-1} owing to the O-H stretching vibration. The peak at 1636 cm^{-1} was given by the stretching vibrations of the C=O groups. The C=N stretching vibration of the azomethine group was found at 1501 cm^{-1} thus, indicating that the ligand formed. The N-H wagging vibration of the secondary amine group, gave a band at 749 cm^{-1} . The N-O stretching vibrations of the $-\text{NO}_2$ group was found at 1356 and 1460 cm^{-1} . The bands at 1189 and 1275 cm^{-1} were given by the two C-O stretching vibrations of the pyrone ring.

In the spectra of the complexes, the bands of the carbonyl and azomethine groups, all experienced a shift in their vibrational frequency. This shows that the carbonyl oxygen and the azomethine nitrogen atoms participated in the coordination. The O-H band was still present in the spectrum of all the complexes indicative of the nonparticipation of the hydroxyl oxygen in the coordination (no deprotonation occurred). The secondary amine band was also found present in the spectra of the complexes which shows that the amine nitrogen did not involve in the coordination. The M-O and M-N vibrational peaks were found in the spectra of the complexes in the range, $416\text{--}443\text{ cm}^{-1}$, and $545\text{--}668\text{ cm}^{-1}$, respectively. This is highly convincing that coordination occurred, adding that these bands were absent in the spectrum of the ligand. For the Cu(II) complex, the M-Cl band was found at 711 cm^{-1} while the peaks

at $3733\text{--}3900\text{ cm}^{-1}$ are due to the coordinated water molecule and hydrogen bonding. Noteworthy of mentioning are the minor peaks found in the spectra of the compounds which are due to bending vibrations. However, other unidentified peaks could have arisen due to overtones. The assignment of these bands was done following literature reports.^[44–49] From the ligand atoms that participated in the coordination, one can point out that the ligand is tridentate. The proposed structures of the complexes are shown in Figure 1.

3.5. Electronic spectra

The electronic spectra (Figure 2a) to an extent, reveal the environment of the ligand as well as the geometry of the complexes. $\pi \rightarrow \pi^*$ and $n \rightarrow \pi^*$ transitions occurred within the ligand at 226.5 nm and 276.5 nm , respectively, owing to the aromatic rings and heteroatoms found in the ligand. The band at 361 nm is attributed to the $n \rightarrow \pi^*$ transition of the azomethine group, indicating that the ligand formed. Again, this transition has experienced a blue shift in the spectrum of all the complexes. This shows that the azomethine nitrogen is involved in coordination in all the complexes. However, this absorption has decreased intensity for the manganese complex, in DMSO, it is the most paramagnetic and has the least ionic radius, but we are unsure which one accounts for this observation.

3.6. UV titrations of the ligand and the complexes

To determine the suitable solvents for UV and NMR analysis the solubility of the compounds were tested. At room temperature compounds were not soluble in H_2O and CCl_3 but were is

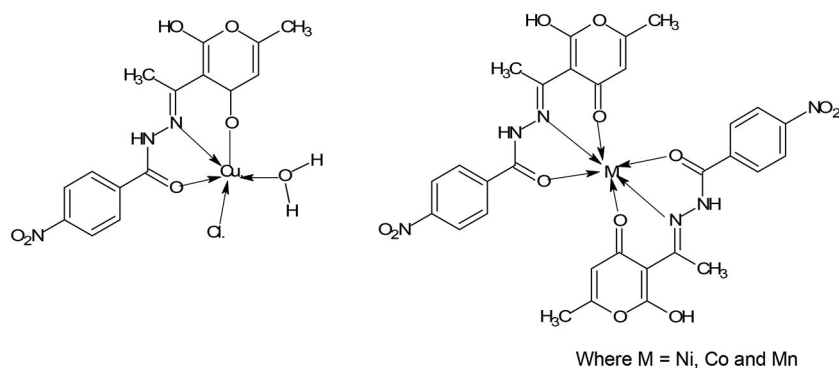


Figure 1. Proposed structures of metal complexes.

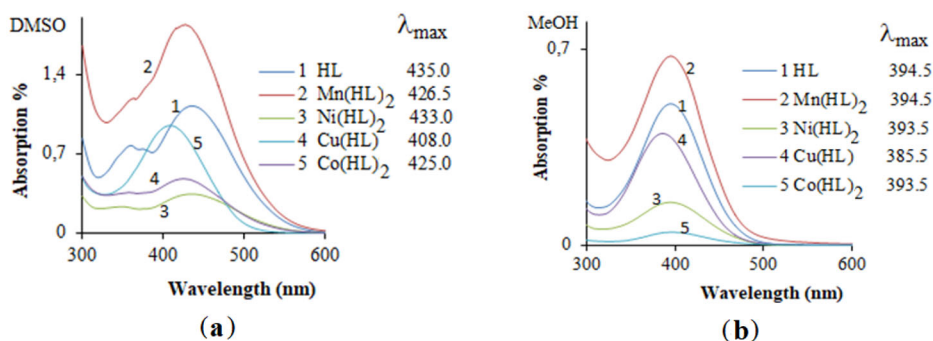


Figure 2. Electronic Spectra of ligand and its complexes showing $\pi \rightarrow \pi^*$ & $n \rightarrow \pi^*$ transitions in DMSO and MeOH.

observed be soluble in MeOH and DMSO. There is no indication that the compounds were not stable in solution. The absorption band of the compounds in DMSO solution is given in Figure 2a. It shows that the ligand (HL) in DMSO has a distinct three-maximal absorption band at 435.0, 375.0, and 276.5 nm. Of these, the electronic transition with λ_{max} at 435.0 nm appears to be the most severe transition by showing a hypochromic shift in the Ni, Mn, Co, and Cu complexes, respectively. The absorption band of the compounds in MeOH solution is given in Figure 2b. While bands were formed as separate maxima of HL and its complexes in DMSO, they formed as a single band in MeOH (Figures 2b). DMSO is more polar than MeOH and is a proton acceptor solution. DMSO can ionize the acidic HL molecule more than MeOH. The difference in the absorption bands of the HL ligand in the two solvents may be due to the difference in polarity (Figures 2a–b). These differences observed for HL are also observed in complexes.

The absorption band of the compounds in MeOH solution upon addition of HCl and KOH is given in Figure 3a–f. While the spectra of HL in MeOH and Methanol + KOH are similar, the spectra in Methanol + HCl are quite different. The fact that HL in MeOH is highly affected by the addition of HCl ($\Delta\lambda_{\text{max}} = 70.0$ nm) and KOH ($\Delta\lambda_{\text{max}} = 0$ nm) indicates that HL is anionic in MeOH (Figure 3a). The fact that HL complexes are affected like HL by the addition of HCl ($\Delta\lambda_{\text{max}} = 23.0$ – 22.5 nm) and KOH ($\Delta\lambda_{\text{max}} = 31.5$ – 16.5 nm) indicates whether HL attached to the complexes has an acidic H atom. In summary, indicating that the bond between the HL ligand and the metal ions is anionic. The addition of HCl caused a hypsochromic shift of about 70 nm (31.5 for Cu) in the complexes, while the addition of KOH caused bathochromic shifts and hyperchromic increases (excluding Cu) between 2.5 and 7 nm.

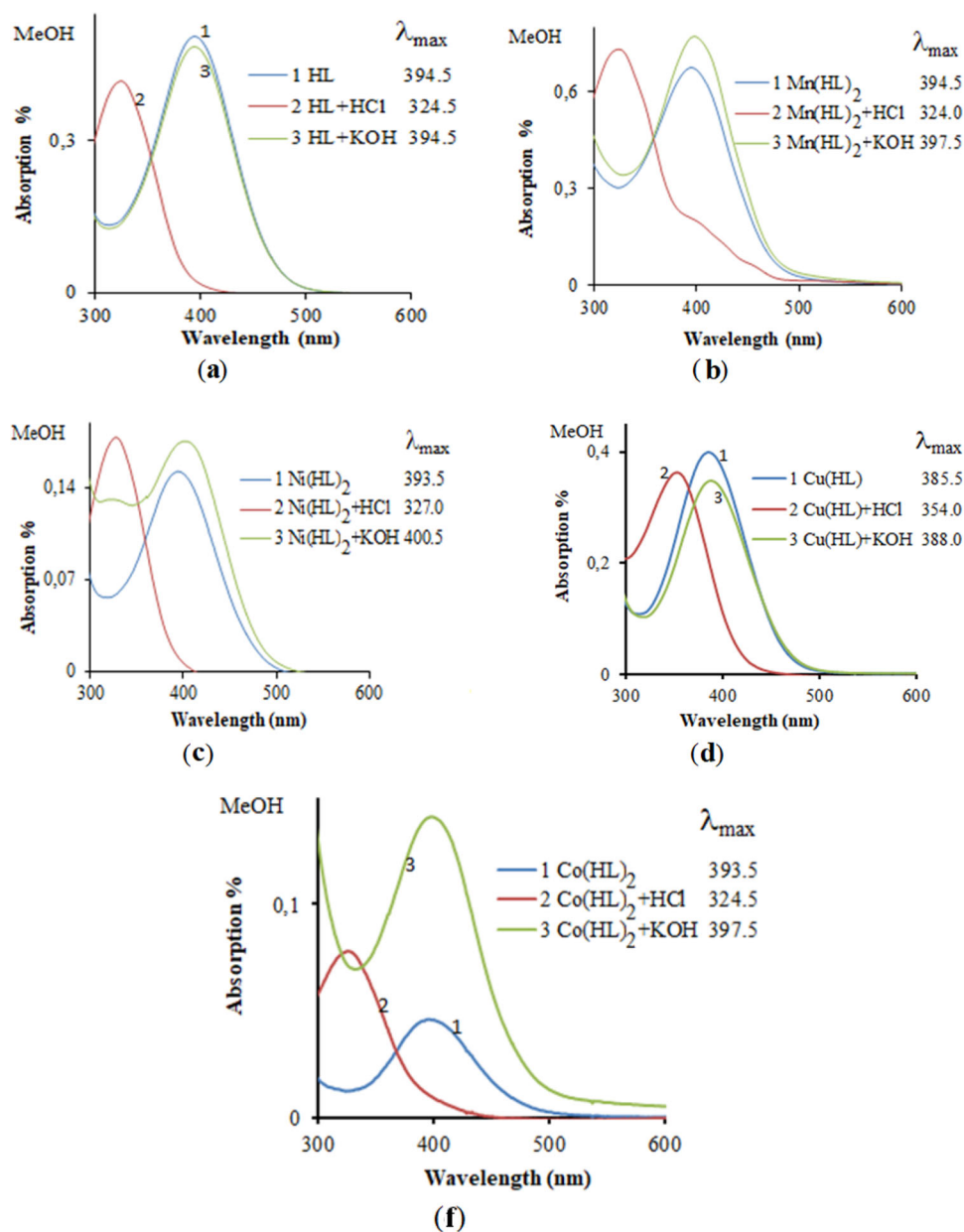


Figure 3. The absorption band of the compounds in DMSO solution (a), in MeOH (b), in MeOH solution with HCl and KOH (3a–f).

Table 1. Antimicrobial activities of compounds (1000 µg/mL) (Inhibition zone mm).

Test microorganisms	Inhibition zones (mm)																
	Compounds					Reference antibiotics											
	HL	Co (HL) ₂	Ni (HL) ₂	Cu HL	Mn (HL) ₂	C 30	CN10	TE 30	E 15	AMP10	P10	K30	OFX5	VA30	CTX30	NS 100	CTL 10
<i>Escherichia coli</i> ATCC 35218	–	–	–	–	–	24	21	15	11	–	16	20	28	23	10	NT	NT
<i>Enterobacter aerogenes</i> ATCC 13048	–	–	–	–	–	19	20	14	–	–	–	–	19	–	20	NT	NT
<i>Salmonella typhimurium</i> ATCC 14028	–	–	–	–	–	17	16	15	8	8	15	18	25	21	13	NT	NT
<i>Micrococcus luteus</i> , ATCC 9341	–	–	–	–	–	25	15	26	30	28	13	12	24	14	17	NT	NT
<i>Staphylococcus aureus</i> ATCC 25923	–	–	–	–	–	23	20	22	23	20	12	13	23	13	12	NT	NT
<i>Staphylococcus epidermidis</i> ATCC 12228	–	–	–	–	–	22	17	19	11	17	11	13	22	12	13	NT	NT
<i>Klebsiella pneumoniae</i> ATCC 13882	–	–	–	–	–	21	19	20	14	–	18	19	27	23	14	NT	NT
<i>Pseudomonas aeruginosa</i> ATCC 35032	–	15	–	–	–	22	20	20	21	–	14	20	29	18	14	NT	NT
<i>Corynebacterium xerosis</i> ATCC 373	–	–	–	9	–	20	17	25	26	27	14	12	22	21	20	NT	NT
<i>Mycobacterium smegmatis</i> ATCC 607	–	–	–	–	–	23	18	26	25	19	16	13	30	20	12	NT	NT
<i>Listeria monocytogenes</i> ATCC 19112	–	–	–	–	–	19	14	12	–	12	10	12	29	25	16	NT	NT
<i>Serratia marcescens</i> ATCC 13880	–	–	–	–	–	23	19	13	–	19	18	19	27	27	13	NT	NT
<i>Proteus vulgaris</i> ATCC 33420	–	–	–	–	–	17	24	16	20	–	15	25	26	24	18	NT	NT
<i>Enterococcus faecalis</i> ATCC 29212	–	–	–	–	–	16	11	19	–	14	12	13	28	20	16	NT	NT
<i>Streptococcus pneumoniae</i> ATCC 27336	–	–	–	–	–	24	20	25	15	14	19	21	28	29	15	NT	NT
<i>Streptococcus mutans</i> **	–	–	–	–	–	28	22	19	–	–	–	22	30	–	22	NT	NT
<i>Bacillus cereus</i> ATCC 11778	–	–	–	–	–	23	24	25	26	–	10	11	28	21	17	NT	NT
<i>Bacillus subtilis</i> ATCC 6633	–	–	–	–	–	22	20	12	25	–	11	11	27	20	16	NT	NT
<i>Candida albicans</i> ATCC 10231	–	12	–	–	–	NT	NT	NT	NT	NT	NT	NT	NT	NT	NT	22	NT
<i>Candida utilis</i> ATCC 9950	–	–	–	–	–	NT	NT	NT	NT	NT	NT	NT	NT	NT	NT	21	NT
<i>Candida tropicalis</i> *	–	–	–	–	–	NT	NT	NT	NT	NT	NT	NT	NT	NT	NT	18	NT
<i>Candida glabrata</i> *	–	–	–	–	–	NT	NT	NT	NT	NT	NT	NT	NT	NT	NT	16	NT
<i>Saccharomyces cerevisiae</i> ATCC 9763	–	–	–	–	–	NT	NT	NT	NT	NT	NT	NT	NT	NT	NT	15	NT
<i>Debaryomyces hansenii</i> NRRL Y-1458	–	–	–	–	–	NT	NT	NT	NT	NT	NT	NT	NT	NT	NT	19	NT
** <i>Torulaspora delbrueckii</i>	–	–	–	–	–	NT	NT	NT	NT	NT	NT	NT	NT	NT	NT	20	NT
** <i>Hansenula philodendron</i>	–	–	–	–	–	NT	NT	NT	NT	NT	NT	NT	NT	NT	NT	22	NT
** <i>Pichia pastoris</i>	–	–	–	–	–	NT	NT	NT	NT	NT	NT	NT	NT	NT	NT	22	NT
** <i>Kluyveromyces fragilis</i>	–	–	–	–	–	NT	NT	NT	NT	NT	NT	NT	NT	NT	NT	20	NT
** <i>Dekkera bruxellensis</i>	–	–	–	–	–	NT	NT	NT	NT	NT	NT	NT	NT	NT	NT	19	NT
* <i>Aspergillus niger</i>	–	–	–	–	–	NT	NT	NT	NT	NT	NT	NT	NT	NT	NT	NT	24
* <i>Aspergillus flavus</i>	–	–	–	–	–	NT	NT	NT	NT	NT	NT	NT	NT	NT	NT	NT	23
* <i>Aspergillus fumigatus</i>	–	–	–	–	–	NT	NT	NT	NT	NT	NT	NT	NT	NT	NT	NT	22
* <i>Aspergillus foetidus</i>	–	–	–	–	–	NT	NT	NT	NT	NT	NT	NT	NT	NT	NT	NT	23

C30: Chloramphenicol (30 mg Oxoid), CN10: Gentamycin (10 mg Oxoid), TE30: Tetracycline (30 mg Oxoid), Kanamisin (30 mg Oxoid), Penicillin (10 mg Oxoid), E15: Erythromycin (15 mg Oxoid), AMP10: Ampicillin (10 mg Oxoid), Ofloxacin (5 mg Oxoid), Vancomycin (30 mg Oxoid), Cefotaxime (30 mg Oxoid), NS: Nystatin (100 mg Oxoid), CLT10: Ketoconazole.

(–): Zone did not occur. NT: Not tested,

(*): Special gift from Aydın Adnan Menderes University Faculty of Medicine.

(**): Special gift from Ege University Faculty of Microbiology Department.

3.7. Antimicrobial analysis

The results of antimicrobial activities of the study compounds and the reference antibiotics reported as inhibition zone diameter (mm) are shown in Table 1. The Minimum

inhibitory concentration (MIC) values which suggested that some of the studied compounds indicated considerable antimicrobial activity are shown in Table 2.

The ligand did not show any antimicrobial activity. However, literature reports indicating that the antimicrobial

activities of hydrazone may be enhanced on complexation are replete in literature.^[50–52] Expectedly, according to Table 1, Co(HL)₂ showed a moderate effect (15–12 mm) against *Pseudomonas aeruginosa* ATCC 35032 and *Candida albicans* ATCC 10231, and Cu(HL) indicated a very low effect (9 mm) against *Corynebacterium xerosis* ATCC 373. However, the

Table 2. Antimicrobial activities of compounds (MIC, $\mu\text{g.mL}^{-1}$).

Test microorganisms	Co(L4) ₂	Cu(L4) ₂	Str	Flk
<i>Pseudomonas aeruginosa</i> ATCC 35032	32	–	64	NT
<i>Corynebacterium xerosis</i> ATCC 373	–	256	64	NT
<i>Candida albicans</i> ATCC 10231	64	–	NT	64

Str: Streptomycin, Flk = Flukanazol.

(–): No effect, NT: Not tested.

Table 3. The half-maximal inhibitory concentration (IC₅₀) values of the compounds against breast (MCF-7) and prostate (PC-3) cancer cells.

Compounds	Cell line	IC ₅₀ ($\mu\text{g/mL}$)
Paclitaxel	MCF-7	18.12 \pm 2.33
	PC-3	16.23 \pm 1.72
Ni(HL) ₂	MCF-7	22.68 \pm 6.26
	PC-3	11.42 \pm 9.06
Co(HL) ₂	MCF-7	22.69 \pm 4.56
	PC-3	9.31 \pm 13.49
Cu(HL)	MCF-7	23.26 \pm 9.66
	PC-3	19.56 \pm 7.17
Mn(HL) ₂	MCF-7	21.94 \pm 13.8
	PC-3	6.52 \pm 34.70

compounds do not affect tested other bacteria, yeasts, and microfungi.

The MIC values in Table 2 also showed that the compounds Co(HL)₂ have remarkable antimicrobial activity (32–64 $\mu\text{g.mL}^{-1}$) on *Pseudomonas aeruginosa* ATCC 35032 and *Candida albicans* ATCC 10231. On the other hand, compound Cu(L4)₂ had a very low effect (256 $\mu\text{g.mL}^{-1}$) on *Corynebacterium xerosis* ATCC 373.

3.8. Anti-proliferative studies

The newly synthesized HL and its metal complexes were tested against two human cancer cell lines (MCF-7 and PC-3) for their cytotoxic and apoptotic effects properties. MCF-7 and PC-3 cells were seeded to 48 and 96-well plates and treated with increasing concentrations of test chemicals. Cell proliferation was calculated using MTT data and from these results, IC₅₀ values were determined.

The antiproliferative effects of the new metal complexes were analyzed and their apoptotic effects were determined with the Hoechst/propidium iodide double staining method in both cancer cell lines. Paclitaxel was used as the positive control (1 μM). The results indicated that the metal complexes are effective on breast cancer (MCF-7) cells in terms of cell death and can stop the growth of these cancer cells.

Cytotoxic effects of drugs on MCF-7 cell line

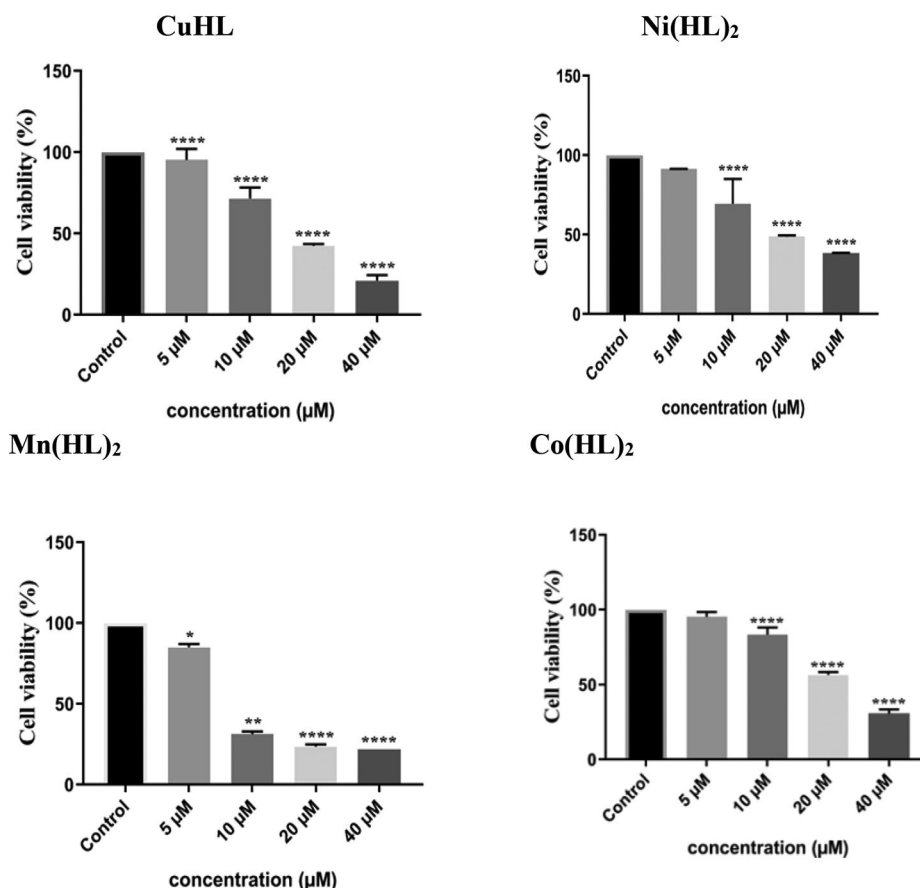


Figure 4. The cytotoxic efficiency of drugs with untreated control groups on MCF-7 cells. The data were represented as mean \pm standard error of the mean. A comparison was performed by The One Way ANOVA test with Dunnett's multiple comparison test was applied as a post-hoc test. p -value equal or less than 0.05 were considered as statistically significant ($+p < 0.05$, $++p < 0.01$, $+++p < 0.001$, $++++p < 0.0001$) versus untreated control.

Cytotoxic effects of drugs on PC3 cell line

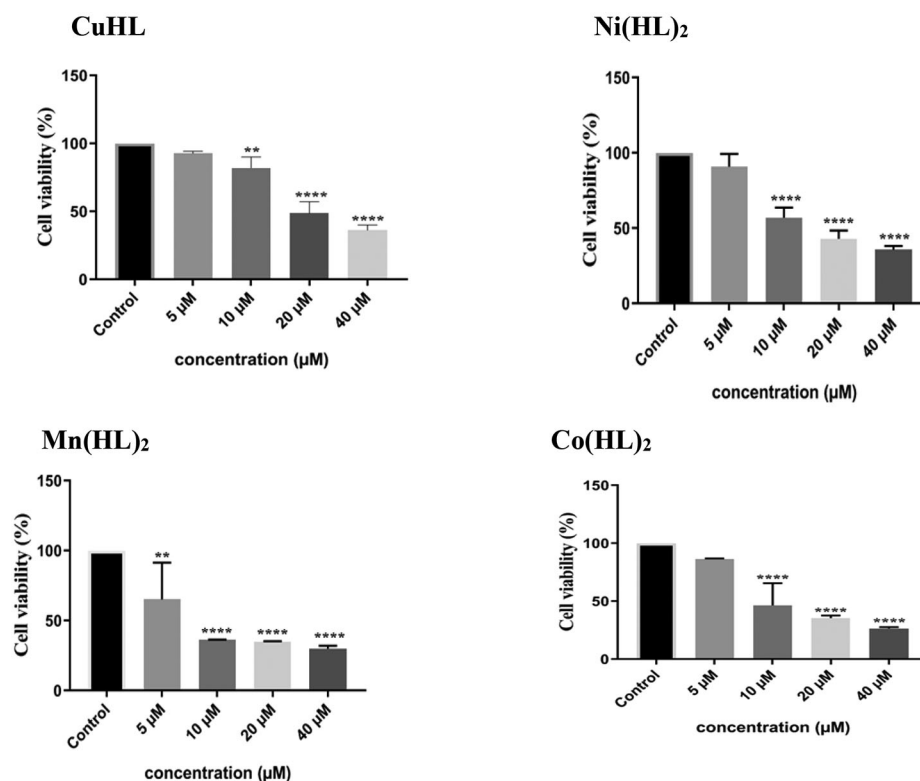


Figure 5. The cytotoxic efficiency of drugs with untreated control groups on PC-3 cells. The data were represented as mean \pm standard error of the mean. A comparison was performed by The One Way ANOVA test with Dunnett's multiple comparison test was applied as a post-hoc test. p -value equal or less than 0.05 were considered as statistically significant (* $p < 0.05$, ** $p < 0.01$, *** $p < 0.001$, **** $p < 0.0001$) versus untreated control.

Table 4. The apoptotic cell values of the compounds against breast (MCF-7) and prostate (PC-3) cancer cells.

Compounds	Cell line	Apoptosis rate \pm S.D
Pax	MCF-7	58.15 \pm 2.11
	PC-3	66.16 \pm 3.75
Ni(HL) ₂	MCF-7	75.65 \pm 2.96
	PC-3	91.72 \pm 2.87
CuHL	MCF-7	79.08 \pm 2.90
	PC-3	74.33 \pm 5.17
Mn(HL) ₂	MCF-7	76.88 \pm 2.85
	PC-3	86.20 \pm 2.00
Co(HL) ₂	MCF-7	87.23 \pm 5.30
	PC-3	86.40 \pm 5.57
Control	MCF-7	9.99 \pm 3.01
	PC-3	10.47 \pm 1.11

In the test results with MCF-7 and PC-3 cell lines, the inhibition concentration for 50% of cells (IC₅₀) was calculated to be about generally 10 μ M. In this study, the metal complexes of the ligand (HL) were determined to have a strong antiproliferative activity, with an IC₅₀ value of μ M for MCF-7 and PC3 cells.

The calculated IC₅₀ values for the molecules are, respectively, Mn(HL)₂ 21.94 μ M, Ni(HL)₂ 22.68, Co(HL)₂ μ M 22.69 and CuHL 23.26 for MCF-7 cell line (Table 3). The calculated IC₅₀ values for the molecules are, respectively, Mn(HL)₂ 6.52 μ M, CoL4 μ M 9.31, Ni(HL)₂ 11.42, and CuHL 19.56 for the PC-3 cell line (Table 3). Especially the effect of Mn(HL)₂ is strong on PC-3 and MCF-7 cell lines.

In comparison with the known drug, Paclitaxel, it can be seen that the activity of the multicomplex molecule against the cancer cell is almost equal to the standard drug. The

Apoptotic and necrotic cells observed after drug application in MCF-7 cell line

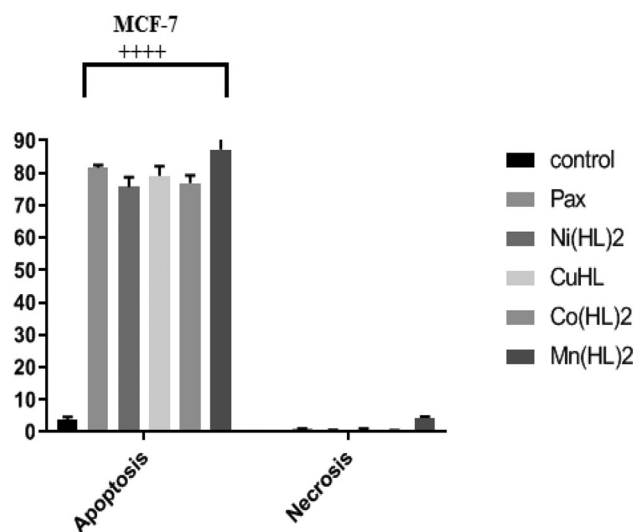


Figure 6. Apoptosis measurement of drugs on MCF-7 cells. The data were represented as mean \pm standard error of mean. Comparison was performed by The One Way ANOVA test with Dunnett's multiple comparison test was applied as a post-hoc test. p -value equal or less than 0.05 were considered as statistically significant (+ $p < 0.05$, ++ $p < 0.01$, +++ $p < 0.001$, ++++ $p < 0.0001$) versus untreated control.

calculated IC₅₀ is 16.23 μ M for Paclitaxel and 6.52 μ M for [Mn(HL)₂] on the PC-3 cell line (Table 3). This is a strong effect for a newly synthesized compound. Similar activity was observed on the MCF-7 cell line. The IC₅₀ values for

Apoptotic and necrotic cells observed after drug application in PC-3 cell line

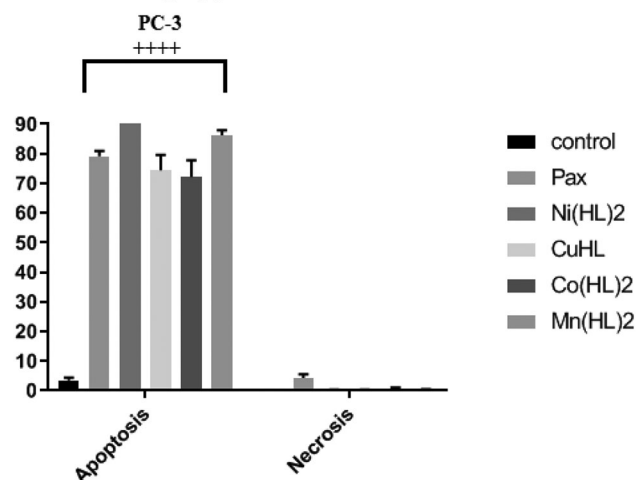


Figure 7. Apoptosis measurement of drugs on PC-3 cells. The data were represented as mean \pm standard error of the mean. A comparison was performed by The One Way ANOVA test with Dunnett's multiple comparison test was applied as a post-hoc test. p -value equal or less than 0.05 were considered as statistically significant (* $p < 0.05$, ** $p < 0.01$, *** $p < 0.001$, **** $p < 0.0001$) versus untreated control.

the MCF-7 cell line were calculated, 18.12 μM for Paclitaxel and 21.94 μM for $[\text{Mn}(\text{HL})_2]$ (Table 3). These results show that the new molecules are generally more effective on PC-3 cell lines. Apart from the strong activity of $[\text{Mn}(\text{HL})_2]$ only the high concentrations of the other compounds were effective on different cell lines. Therefore, it can be suggested that these newly synthesized compounds, especially $[\text{Mn}(\text{HL})_2]$, are potent candidates against prostate cancer cells (PC-3) and should be considered in more detailed studies as anti-cancer agents.

Analysis of the type of cell death indicated a great rate of apoptosis in 24 h. The results were compatible with proliferation data and the cells died after 24 h by apoptotic mechanisms. The apoptotic and necrotic cell values of the compounds against breast (MCF-7) and prostate (PC-3) cancer cells are given in Figures 4 and 5 and Tables 3 and 4. These important results for the MCF-7 and PC-3 cell lines give us information about the effectiveness of the newly synthesized products. If the results are compared with the familiar drug paclitaxel (1 μM), we can see that our products, especially $\text{Mn}(\text{HL})_2$, $\text{Co}(\text{HL})_2$, and $\text{Cu}(\text{HL})_2$ complexes, can compete with this drug.

Analysis of the type of cell death indicated a great rate of apoptosis in 24 h. The results were compatible with proliferation data and the cells died after 24 h by apoptotic mechanisms. The apoptotic and necrotic cell values of the compounds against breast (MCF-7) and prostate (PC-3) cancer cells are given in Figures 6 and 7.

3.9. Theoretical considerations

3.9.1. Theoretical calculations of infrared spectra

Figure 8 presents the calculated infrared spectra of HL and $\text{Mn}(\text{HL})_2$ complex while Table 5 shows the comparison of selected experimental infrared spectra of HL and $\text{Mn}(\text{HL})_2$

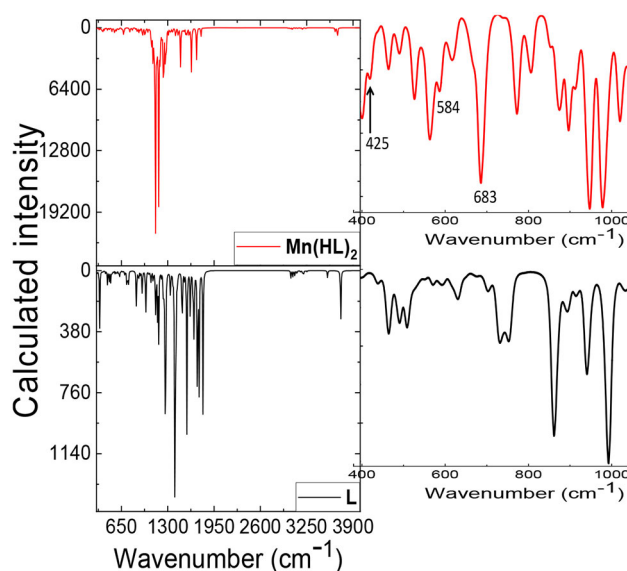


Figure 8. Infrared spectra of ligand and complex calculated at B3LYP/6-31G(d) and B3LYP/SDD, respectively.

Table 5. Selected experimental and calculated infrared spectra data for ligand and complexes (DFT calculated in vacuum at B3LYP/6-31G(d) for HL and at B3LYP/SDD for $\text{Mn}(\text{HL})_2$).

Assignment (cm^{-1})	HL		$\text{Mn}(\text{HL})_2$	
	Experiment	DFT	Experiment	DFT
$\nu(\text{O-H})$	3435	3728	3444	3681
$\nu(\text{C=O})$	1637	1717, 1795	1635	1631
$\nu(\text{C=N})$	1501	1503, 1569	1547	1535
$\nu(\text{N-O})$	1460, 1356	1398	—	—
$\nu(\text{C-O})$	1275, 1189	1271	—	—
$\nu(\text{N-H})$	749	742	749	737
$\nu(\text{M-O})$	—	—	—	681, 683
$\nu(\text{M-N})$	—	—	587	584
$\nu(\text{M-O})$	—	—	420	425

complex and calculated data in gas phase. There is good agreement between theory and experiment, Table 5. The shift in the $\nu(\text{C=O})$ of the ligand upon coordination to the metal center is pronounced in both the experiment and the theoretical assignments. As expected there is a shift from higher vibrational energy 1637 (1717) cm^{-1} in the ligand to lower vibrational energy 1635 (1631) cm^{-1} in the metal complex. Strikingly, calculated vibrational signals at 425 and 683 cm^{-1} , ascribed to Mn-O, are observed in experimental data at 420 and 587 cm^{-1} , these are absent in HL infrared spectrum and this shows that metal complex coordinated to the ligand atoms.

3.9.2 Theoretical calculations of uv-visible spectra

Figure 9 compares the calculated absorption spectra of HL and experimental data in methanol solvent. From the spectra data in Figure 9, the calculated spectra comparatively gave good descriptions of the experimental spectra. The agreement between the calculated and experimental data for HL in methanol/KOH (Figure 9a and b) confirmed the proposed structure in Scheme 2. Figure 10 presents the optimized geometries for the proposed HL conformations in methanol/KOH (Figure 10a), in methanol only (Figure 10b) and in methanol/HCl (Figure 10c). Of the proposed HL

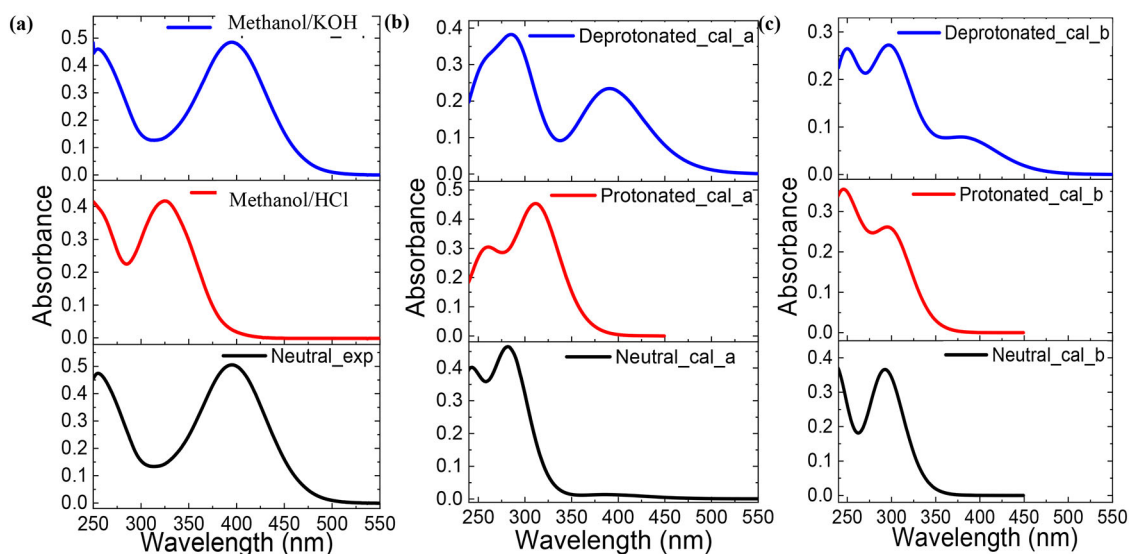
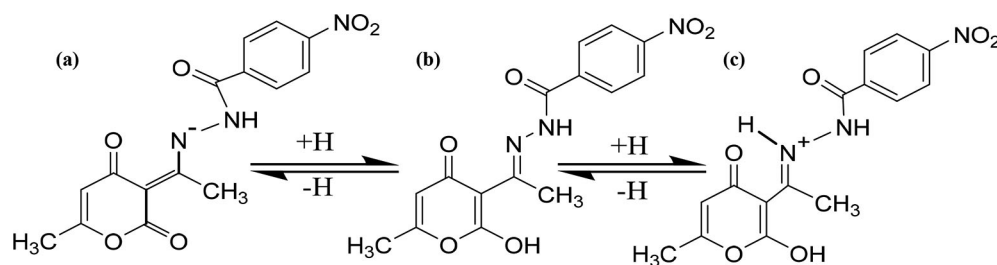


Figure 9. Experiment and calculated (B3LYP/6-31G(d)) UV-visible spectra of ligand.



Scheme 2. Proposed structures of HL in acidic, basic and neutral solutions

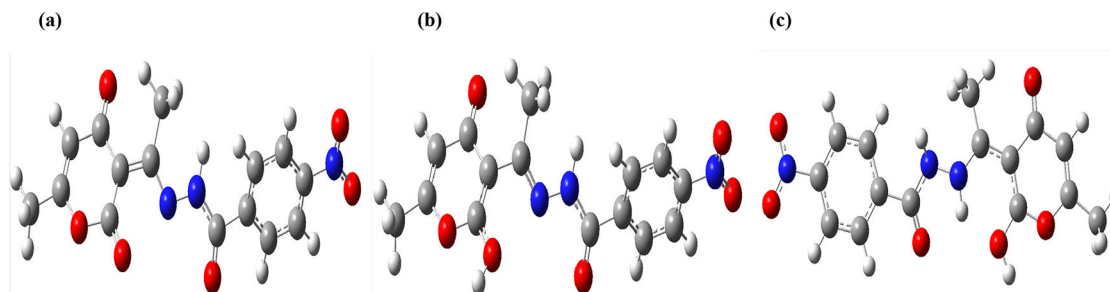
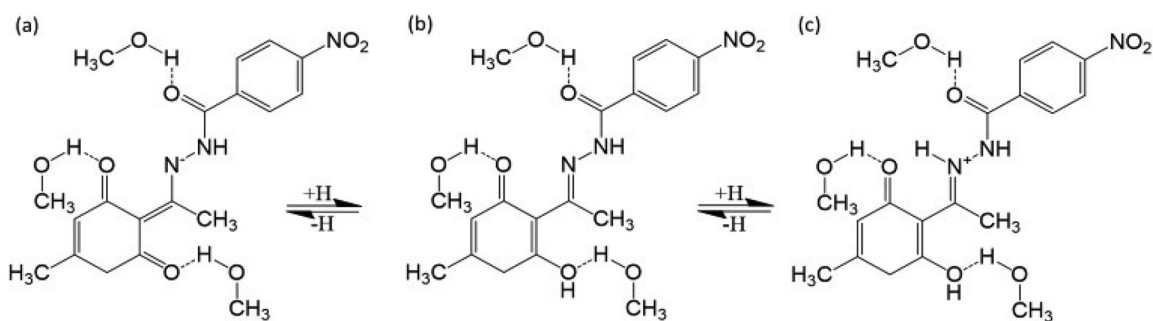


Figure 10. Proposed structures showing optimized graphics of (a) HL in methanol containing KOH (deprotonated), (b) HL in methanol and (c) HL in methanol containing HCl (protonated), at B3LYP/6-31(D).



Scheme 3. Proposed structures of methanol solvated HL in acidic, basic and neutral solutions

conformations, Figure 10a shows the most probable conformation of HL in methanol/KOH which gave rise to calculated uv-vis spectrum designated deprotonated_cal_a (Figure 9b). Theoretical calculation therefore suggests that HL

became deprotonated in methanol when KOH was added (Scheme 2a).

Observation shows that the calculated spectra, Figure 9a and c, agrees well with the experimental spectra for HL in

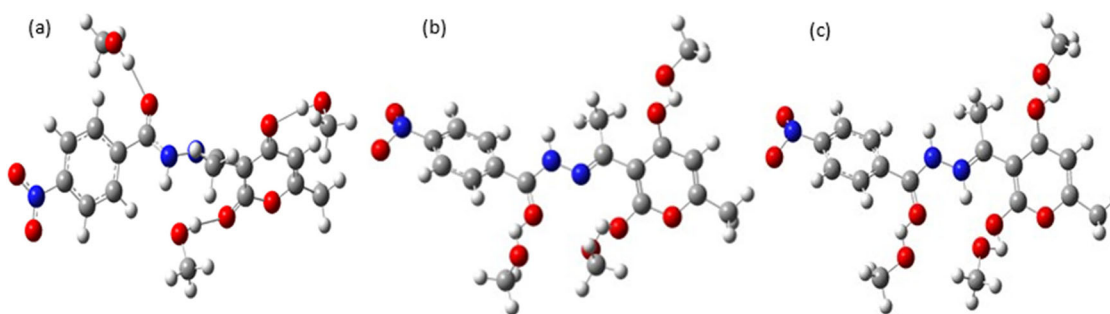


Figure 11. Proposed structures showing optimized graphics of methanol solvated (a) HL in methanol containing KOH (deprotonated), (b) HL in methanol and (c) HL in methanol containing HCl (protonated), at B3LYP/6-31(D), revealing hydrogen bonded methanol molecules.

Table 6. Quantum chemical parameters performed in gas at B3LYP/6-31(d) for HL and B3LYP/SDD for the complexes.

	E_{HOMO} (eV)	E_{LUMO} (eV)	ΔE (eV)	χ (eV)	η	δ
HL	-5.714	-3.120	2.594	4.417	1.297	0.771
Co(HL) ₂	-4.041	-3.309	0.733	3.675	0.366	2.729
CuHL	-5.962	-3.788	2.173	4.875	1.087	0.920
Mn(HL) ₂	-4.038	-3.549	0.489	3.794	-0.245	-4.088
Ni(HL) ₂	-3.830	-3.364	0.466	3.597	-0.233	-4.296

methanol and HL in methanol/HCl, and suggest strongly the proposed structures, Scheme 3b and c. From theoretical calculations it can be observed that HL not only became protonated in methanol when HCl was added, hydrogen bonded methanol molecules at sites available in HL are possible as proposed in Scheme 3b and c. Figure 11 presents the optimized geometries for the proposed HL conformations in methanol (Figure 11b) and in methanol/HCl (Figure 11c). Among the proposed HL conformations, Figure 11b and c show the most probable conformations of HL in methanol alone and in methanol/KOH which gave rise to calculated uv-vis spectra, respectively, designated neutral_cal_b and protonated_cal_b (Figure 9c).

3.9.3. Theoretical considerations of antimicrobial activities

Table 6 presents the molecular parameters from theoretical calculations for the studied inhibitor molecules. Earlier work^[2] reported calculations of the following, energy gap ($E = E_{\text{LUMO}} - E_{\text{HOMO}}$), global hardness (η) and global electronegativity (χ), Eqs. (1)–(3), as vital parameters for molecular descriptions.

$$\chi \cong -1/2 (E_{\text{HOMO}} + E_{\text{LUMO}}) \quad (1)$$

$$\eta \cong -1/2 (E_{\text{HOMO}} - E_{\text{LUMO}}) \quad (2)$$

$$\sigma = 1/\eta \cong -2/(E_{\text{HOMO}} - E_{\text{LUMO}}) \quad (3)$$

where E_{HOMO} and E_{LUMO} , respectively, are energy of the highest occupied molecular orbitals and energy of the lowest unoccupied molecular orbitals.

Explanation of molecular reactivities using computational techniques are known.^[2] Figure 12 reveals that the ligand has its HOMO and LUMO around the (E)-N'-(1-(2-hydroxy-4-oxo-4H-pyran-3-yl)ethylidene)acetohydrazide region. This is to say that for the ligand, HL, electron distributions in the (E)-N'-(1-(2-hydroxy-4-oxo-4H-pyran-3-

yl)ethylidene)acetohydrazide region are responsible for its antimicrobial activity. The copper complex, CuHL, the region containing copper, water and (E)-N'-(1-(2,4-dihydroxy-6-methyl-4H-pyran-3-yl)ethylidene)formohydrazide consist the HOMO and LUMO, such that the electron distribution around copper dominates the HOMO. The rest complexes, Co(HL)₂, Mn(HL)₂ and Ni(HL)₂, have the (E)-N'-(1-(2,4-dihydroxy-6-methyl-4H-pyran-3-yl)ethylidene)-formohydrazide and the central metals involved in the HOMO and LUMO, such that the electron distribution around central metal dominates the HOMO. Herein, principal component analysis was used to ascertain/determine the molecular parameters from DFT calculations that give best description for the antimicrobial activities of the studied compounds.

3.9.4. Principal component analysis (PCA)

Experimental results reveal that the metal complexes performed better, therefore, the molecular parameters from quantum chemical calculations were subjected to principal component analysis (Table 7). There are six molecular parameters calculated for the studied compounds and on scaling down, only two components are selected using PCA (Table 8). The principal component plots (in rotated spaces) is presented in Figure 13, two factors which account for about 67% and 99% of the total variance in the data are further explained in the rotated component matrix, Table 9. Results of the rotated component matrix reveal that E_{LUMO} and global softness (δ) are the most correlated parameters for components 1 and 2, respectively. PCA therefore suggests that E_{LUMO} and δ would sufficiently account for the observed antimicrobial results of the complexes studied.

Lower values of E_{LUMO} are reported to enhance molecular reactivities/interactions.^[21,24] Values of E_{LUMO} presented in Table 7 show that copper complex has the lowest and accounts for the observed activity against *Corynebacterium xerosis* (Tables 1 and 2).

Similarly, global softness (δ) can be used to describe relative molecular reactivity.^[41,53] Results presented in Table 1 show that activities against *Pseudomonas aeruginosa* and *Candida albicans*, respectively, by cobalt complex, and copper complex was active against *Corynebacterium xerosis*. It is known that higher value of δ translates to better activity as reported elsewhere,^[41,53] therefore calculated higher values

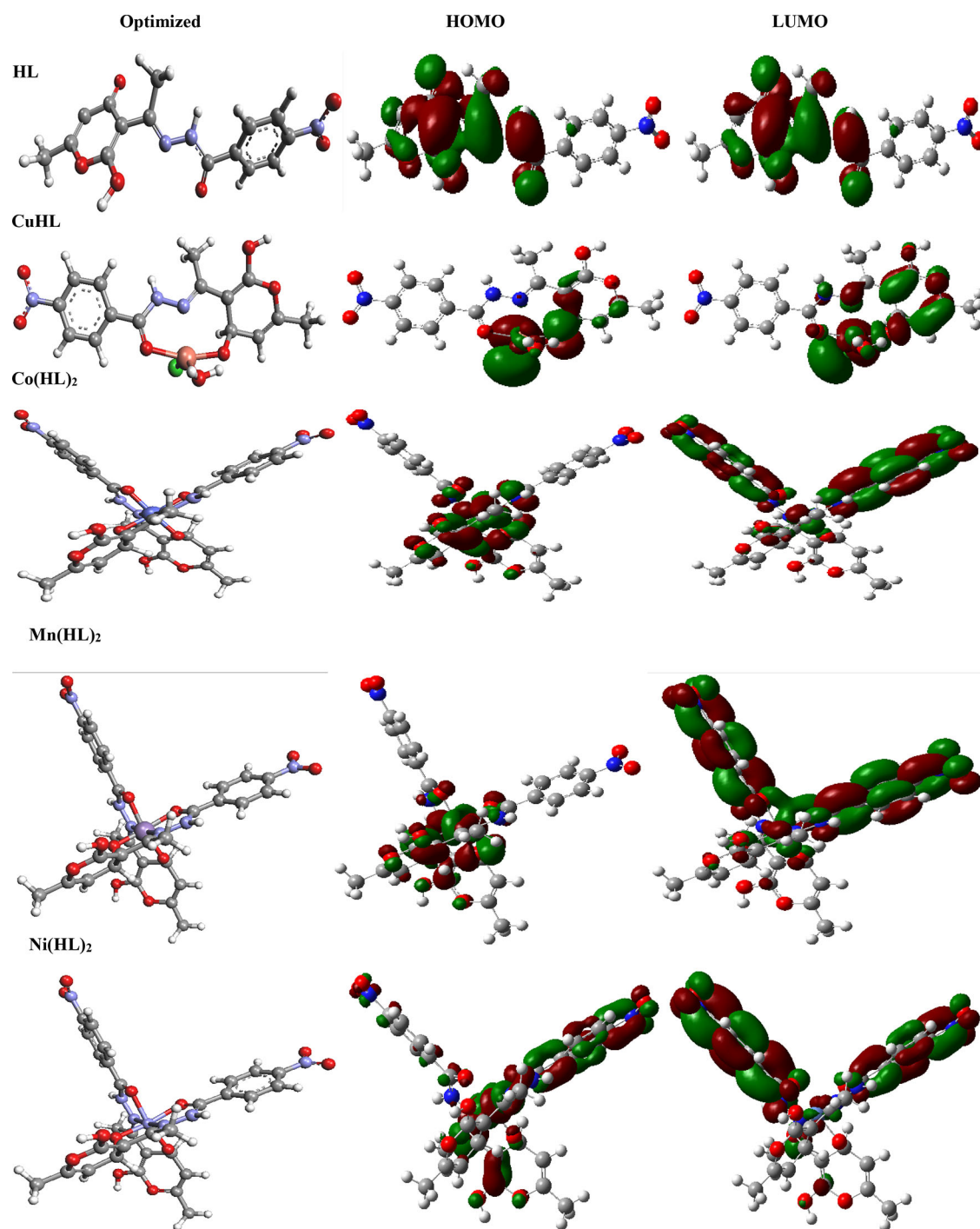


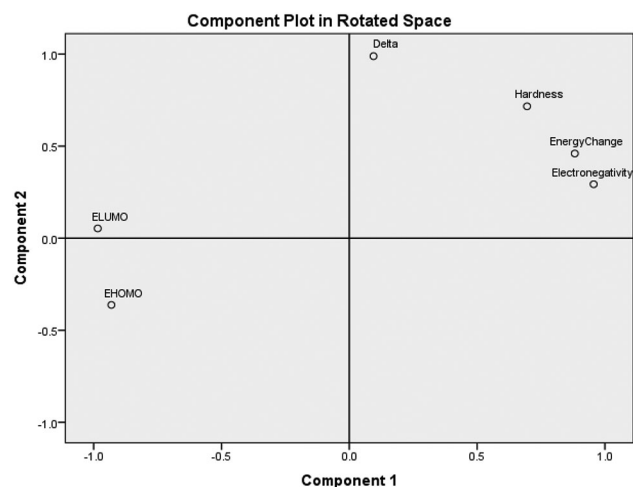
Figure 12. Optimized structures of studied compounds (left) and plots of HOMO (middle) and LUMO (right).

Table 7. Principal component analysis of the explained total variance.

Component	Initial eigenvalues			Extraction sums of square loadings			Rotation sums of square loadings		
	Total	% of variance	Cumulative %	Total	% of variance	Cumulative %	Total	% of variance	Cumulative %
1	4.853	80.892	80.892	4.853	80.892	80.892	4.020	66.999	66.999
2	1.089	18.149	99.041	1.089	18.149	99.041	1.922	32.041	99.040
3	0.058	0.96	100.000						
4	2.710E-16	4.51E-15	100.000						
5	7.820E-17	1.30E-15	100.000						
6	-1.160E-17	-1.93E-16	100.000						

Table 8. Rotated component matrix.

	Component	
	1	2
E_{LUMO}	−0.984	0.053
χ	0.956	0.293
E_{HOMO}	−0.931	−0.362
ΔE	0.882	0.460
δ	0.095	0.989
η	0.695	0.715

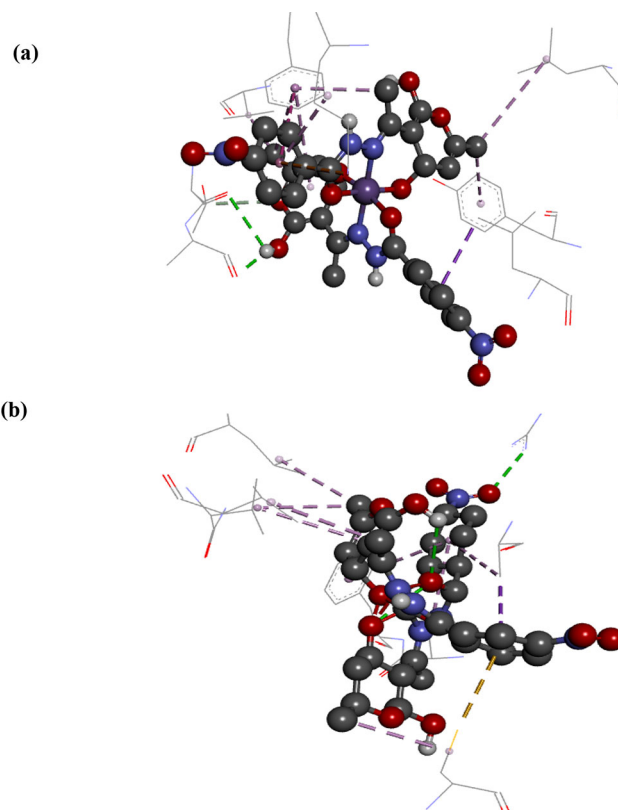
**Figure 13.** Principal component plots in rotated spaces the complexes.**Table 9.** Binding energies from molecular docking results.

Compound	Binding energy (kJ.mol ^{−1})	
	1FDW	3RUK
HL	−28.12	−41.42
CuHL	−31.92	−44.51
Co(HL) ₂	−38.66	−32.97
Mn(HL) ₂	−41.25	−35.40
Ni(HL) ₂	−46.15	−35.23
Paclitaxel	−36.53	−7.82

of δ (Table 7) accounts for the observed antimicrobial activities for cobalt and copper complexes (Tables 1 and 2).

3.9.5. Theoretical considerations of anticancer activities

Molecular docking results are presented in terms of binding energies (Table 9) and protein/ligand interactions (Figure 14). Binding energy results show that the complexes performed better than the ligand for activity against breast cancer, this is consistent with experimental results. The largest binding energy magnitude suggests nickel complex has most activity than the rest complexes, however this is not the case, because it contrasts experimental findings that Mn(HL)₂ performed best. Interestingly DFT comes to rescue. As described above for the use of PCA in the selection of molecular parameters from DFT calculation for antibacterial activities, similarly lower E_{LUMO} value accounts for stronger binding interactions, hence, more activity of Mn(HL)₂ than its nickel counterpart against breast and prostate cancers.

**Figure 14.** Predicted interactions of Mn(HL)₂ with (a) 1FDW (breast cancer) and (b) 3RUK (prostate cancer).

4. Conclusion

Among the compounds under investigation, Co(HL)₂ compound was found to be moderately effective on both *Pseudomonas aeruginosa* ATCC 35032 and *Candida albicans* ATCC 10231, While, the other compounds displayed no effect against the test microorganisms. Cytotoxic and apoptotic effects activities were tested using breast (MCF-7) and prostate (PC-3) cancer cells. The results indicated that the newly synthesized compounds are effective on both prostate and breast cell lines at concentrations between 5 and 40 μM , and exhibit their effects by apoptotic mechanisms. Especially, Mn(HL)₂ could be a potential candidate against prostate cancer cells (PC-3). The theoretical calculations, TD-DFT, gave similar electronic spectra with those of experiment and predict the conformations of HL in methanol, methanol/HCl and methanol/KOH solutions. Molecular docking with the aid of artificial neural network, predicts Mn(HL)₂ as the compound that has most anti-bacteria and anti-cancer activities. This prediction is in excellent agreement with experimental findings.

Acknowledgments

The authors thank the University of Nigeria, Nsukka, Nnamdi Azikiwe University Awka, and Aydin Adnan Menderes University Turkey for infrastructural support.

ORCID

Oguejiofo T. Ujam  <http://orcid.org/0000-0002-5628-209X>

References

- Cassell, G. H.; Mekalanos, J. Development of Antimicrobial Agents in the Era of New and Reemerging Infectious Diseases and Increasing Antibiotic Resistance. *JAMA*. **2001**, *285*, 601–605. DOI: [10.1001/jama.285.5.601](https://doi.org/10.1001/jama.285.5.601).
- Ugwu, N. F.; Anarado, C. J. O.; Ibeji, C. U.; Okpareke, O. C.; Ezeorah, C. J.; Okagu, O. D.; Ekennia, A. C.; Cömert, F.; Babahan, I.; Coban, B.; Ujam, O. T. Synthesis, Spectroscopic, Antimicrobial Activity and Computational Studies of Some Homoleptic and Heteroleptic Metal (II) Complexes of 2-Furoic Acid Hydrazone. *ChemistrySelect*. **2019**, *4*, 11206–11212. DOI: [10.1002/slct.201902870](https://doi.org/10.1002/slct.201902870).
- Popiolek, L. Hydrazide-Hydrazones as Potential Antimicrobial Agents: Overview of the Literature Since 2010. *Med. Chem. Res.* **2017**, *26*, 287–301. DOI: [10.1007/s00044-016-1756-y](https://doi.org/10.1007/s00044-016-1756-y).
- Pandey, A.; Dewangan, D.; Verma, S.; Mishra, A.; Dubey, R. D. Synthesis of Schiff Bases of 2-Amino-5-Aryl-1, 3,4-Thiadiazole and Its Analgesic, anti-Inflammatory, anti-Bacterial and anti-Tubercular Activity. *Inter. J. ChemTech Res.* **2011**, *3*, 178–184.
- Nirmal, R.; Prakash, C.; Meenakshi, K.; Shanmugapandian, P. Synthesis Pharmacological Evaluation of Novel Schiff Base Analogues of 3-(4-Amino) Phenylimino) 5-Fluoroindolin-2-One. *J. Young Pharm.* **2010**, *2*, 162–168. DOI: [10.4103/0975-1483.63162](https://doi.org/10.4103/0975-1483.63162).
- Hussain, I.; Ali, A. Exploring the Pharmacological Activities of Hydrazone Derivatives: A Review. *J. Phytochem. Biochem.* **2017**, *1*, 104.
- Saini, R. P.; Kumar, V.; Gupta, A. K.; Gupta, G. K. Synthesis, Characterization, and Antibacterial Activity of a Novel Heterocyclic Schiff's Base and Its Metal Complexes of First Transition Series. *Med. Chem. Res.* **2014**, *23*, 690–698. DOI: [10.1007/s00044-013-0657-6](https://doi.org/10.1007/s00044-013-0657-6).
- Kargar, H.; Fallah-Mehrjardi, M.; Behjatmanesh-Ardakani, R.; Munawar, K. S.; Ashfaq, M.; Tahir, M. N. Diverse Coordination of Isoniazid Hydrazone Schiff Base Ligand towards Iron (III): Synthesis, Characterization, SC-XRD, HSA, QTAIM, MEP, NCI, NBO and DFT Study. *J. Mol. Struct.* **2022**, *1250*, 131691. DOI: [10.1016/j.molstruc.2021.131691](https://doi.org/10.1016/j.molstruc.2021.131691).
- Kargar, H.; Nateghi-Jahromi, M.; Fallah-Mehrjardi, M.; Behjatmanesh-Ardakani, R.; Munawar, K. S.; Ali, S.; Ashfaq, M.; Tahir, M. N. Synthesis, Spectral Characterization, Crystal Structure and Catalytic Activity of a Novel Dioxomolybdenum Schiff Base Complex Containing 4-Aminobenzhydrazone Ligand: A Combined Experimental and Theoretical Study. *J. Mol. Struct.* **2022**, *1249*, 131645. DOI: [10.1016/j.molstruc.2021.131645](https://doi.org/10.1016/j.molstruc.2021.131645).
- Kargar, H.; Fallah-Mehrjardi, M.; Behjatmanesh-Ardakani, R.; Munawar, K. S. Synthesis, Spectra (FT-IR, NMR) Investigations, DFT, FMO, MEP, NBO Analysis and Catalytic Activity of MoO₂(VI) Complex with ONO Tridentate Hydrazone Schiff Base Ligand. *J. Mol. Struct.* **2021**, *1245*, 131259. DOI: [10.1016/j.molstruc.2021.131259](https://doi.org/10.1016/j.molstruc.2021.131259).
- Kargar, H.; Fallah-Mehrjardi, M.; Behjatmanesh-Ardakani, R.; Munawar, K. S.; Ashfaq, M.; Tahir, M. N. Titanium(IV) Complex Containing ONO-Tridentate Schiff Base Ligand: Synthesis, Crystal Structure Determination, Hirshfeld Surface Analysis, Spectral Characterization, Theoretical and Computational Studies. *J. Mol. Struct.* **2021**, *1241*, 130653. DOI: [10.1016/j.molstruc.2021.130653](https://doi.org/10.1016/j.molstruc.2021.130653).
- Kargar, H.; Torabi, V.; Akbari, A.; Behjatmanesh-Ardakani, R.; Sahraei, A.; Tahir, M. N. Pd(II) and Ni(II) Complexes Containing an Asymmetric Schiff Base Ligand: Synthesis, x-Ray Crystal Structure, Spectroscopic Investigations and Computational Studies. *J. Mol. Struct.* **2020**, *1205*, 127642. DOI: [10.1016/j.molstruc.2019.127642](https://doi.org/10.1016/j.molstruc.2019.127642).
- Rad, F. V.; Housaindokht, M. R.; Jalal, R.; Hosseini, H. E.; Doghaei, A. V.; Goghari, S.; S. Spectroscopic and Molecular Modeling Based Approaches to Study on the Binding Behavior of DNA with a Copper (II) Complex. *J. Fluoresc.* **2014**, *24*, 1225–1234. DOI: [10.1007/s10895-014-1405-0](https://doi.org/10.1007/s10895-014-1405-0).
- Sathyaraj, G.; Weyhermüller, T.; Nair, B. U. Synthesis, Characterization and DNA Binding Studies of New Ruthenium(II)Bisterpyridine Complexes. *Eur. J. Med. Chem.* **2010**, *45*, 284–291. DOI: [10.1016/j.ejmech.2009.10.008](https://doi.org/10.1016/j.ejmech.2009.10.008).
- Mukherjee, A.; Lavery, R.; Bagchi, B.; Hynes, J. T. On the Molecular Mechanism of Drug Intercalation into DNA: A Simulation Study of the Intercalation Pathway, Free Energy, and DNA Structural Changes. *J. Am. Chem. Soc.* **2008**, *130*, 9747–9755. DOI: [10.1021/ja8001666](https://doi.org/10.1021/ja8001666).
- Selvaganapathy, M.; Raman, N. Pharmacological Activity of a Few Transition Metal Complexes: A Short Review. *J. Chem. Biol. Ther.* **2016**, *01*, 2. DOI: [10.4172/2572-0406.1000108](https://doi.org/10.4172/2572-0406.1000108).
- Spaczynska, E.; Mrozek-Wilczkiewicz, A.; Malarz, K.; Kos, J.; Gonec, T.; Oravec, M.; Gawrecki, R.; Bak, A.; Dohanosova, J.; Kapustikova, I.; et al. Design and Synthesis of Anticancer 1-Hydroxynaphthalene-2-Carboxanilides with a p53 Independent Mechanism of Action. *Sci. Rep.* **2019**, *9*, 6387. DOI: [10.1038/s41598-019-42595-y](https://doi.org/10.1038/s41598-019-42595-y).
- Veclani, D.; Tolazzi, M.; Cerón-Carrasco, J. P.; Melchior, A. Intercalation Ability of Novel Monofunctional Platinum Anticancer Drugs: A Key Step in Their Biological Action. *J. Chem. Inf. Model.* **2021**, *61*, 4391–4399. DOI: [10.1021/acs.jcim.1c00430](https://doi.org/10.1021/acs.jcim.1c00430).
- Sharma, D.; Shandilya, P.; Saini, N. K.; Singh, P.; Thakur, V. K.; Saini, R. V.; Mittal, D.; Chandan, G.; Saini, V.; Saini, A. K. Insights into the Synthesis and Mechanism of Green Synthesized Antimicrobial Nanoparticles, Answer to the Multidrug Resistance. *Mat. Today Chem.* **2021**, *19*, 100391. DOI: [10.1016/j.mtchem.2020.100391](https://doi.org/10.1016/j.mtchem.2020.100391).
- Casida, M. E. Time-Dependent Density-Functional Theory for Molecules and Molecular Solids. *J. Mol. Struct. THEOCHEM.* **2009**, *914*, 3–18. DOI: [10.1016/j.theochem.2009.08.018](https://doi.org/10.1016/j.theochem.2009.08.018).
- Serafim, M. M.; Kronenberger, T.; Oliveira, P. R.; Poso, A.; Honório, K. M.; Mota, B. E. F.; Maltarollo, V. G. The Application of Machine Learning Techniques to Innovative Antibacterial Discovery and Development. *Expert. Opin. Drug Discov.* **2020**, *15*, 1165–1180. DOI: [10.1080/17460441.2020.1776696](https://doi.org/10.1080/17460441.2020.1776696).
- Dorović, J.; Marković, Z.; Petrović, Z. D.; Simijonović, D.; Petrović, V. P. Theoretical Analysis of the Experimental UV-Vis Absorption Spectra of Some Phenolic Schiff Bases. *Mol. Phys.* **2017**, *115*, 2460–2468. DOI: [10.1080/00268976.2017.1324183](https://doi.org/10.1080/00268976.2017.1324183).
- Markovic, S.; Tošovic, J. Application of Time-Dependent Density Functional and Natural Bond Orbital Theories to the uv-Vis Absorption Spectra of Some Phenolic Compounds. *J. Phys. Chem. A*. **2015**, *119*, 9352–9362. DOI: [10.1021/acs.jpca.5b05129](https://doi.org/10.1021/acs.jpca.5b05129).
- Durrant, J. D.; Amaro, R. E. Machine-Learning Techniques Applied to Antibacterial Drug Discovery. *Chem. Biol. Drug Des.* **2015**, *85*, 14–21. DOI: [10.1111/cbdd.12423](https://doi.org/10.1111/cbdd.12423).
- Patiny, L.; Borel, A. ChemCalc: A Building Block for Tomorrow's Chemical Infrastructure. *J. Chem. Inf. Model.* **2013**, *53*, 1223–1228. DOI: [10.1021/ci300563h](https://doi.org/10.1021/ci300563h).
- Coughlan, N. J. A.; Henderson, W. Towards the Water Solubilization of [Pt2(μ-S)₂(PPh₃)₄] Derivatives by Polyether Functionalization – A Synthetic and Mass Spectrometric Investigation. *J. Coord. Chem.* **2014**, *67*, 3987–4002. DOI: [10.1080/00958972.2014.893432](https://doi.org/10.1080/00958972.2014.893432).
- Çoban, E. P.; Ertuğrul, E.; Fırıncı, R.; Bıyık, H.; Günay, M. E. Effects of Novel Silver (I) N-Heterocyclic Carbene Complexes on Mycotoxin Producing Fungi and Biofilm Forming Microorganisms. *Drug Discover.* **2021**, *15*, 52–62.
- Oyeka, E. E.; Babahan, I.; Eboma, B.; Ifeanyieze, K. J.; Okpareke, O. C.; Coban, E. P.; Özmen, A.; Coban, B.; Aksel, M.; Özdemir, N.; et al. Biologically Active Acylthioureas and Their Ni(II) and Cu(II) Complexes: Structural, Spectroscopic, anti-Proliferative, Nucleolytic and Antimicrobial Studies. *Inorg. Chim. Acta.* **2021**, *528*, 120590. DOI: [10.1016/j.ica.2021.120590](https://doi.org/10.1016/j.ica.2021.120590).
- Clinical and Laboratory Standards Institute. *Method for Antifungal Disk Diffusion Susceptibility Testing of Yeasts*,

- Approved Guideline, 2nd ed.; Clinical and Laboratory Standards Institute: Wayne, USA, **2004**.
30. Clinical and Laboratory Standards Institute. *CLSIM02-A12: Performance Standards for Antimicrobial Disk Susceptibility Tests: Approved Standard*, 12th ed.; Clinical and Laboratory Standards Institute: Wayne, USA, **2015**.
 31. European Committee on Antimicrobial Susceptibility Testing. *Disk Diffusion Method for Antimicrobial Susceptibility Testing-Version 7.0*. European Society of Clinical Microbiology and Infectious Diseases: Basel, **2019**.
 32. Jorgensen, J. H.; Ferraro, M. J. Antimicrobial Susceptibility Testing: A Review of General Principles and Contemporary Practices. *Clin Infect Dis.* **2009**, *49*, 1749–1755. DOI: [10.1086/647952](https://doi.org/10.1086/647952).
 33. Clinical and Laboratory Standards Institute. *M07–A8: Methods for Dilution Antimicrobial Susceptibility Testing for Bacteria That Grow Aerobically: Approved Standard*, 8th ed.; Clinical and Laboratory Standards Institute: Wayne, USA, **2009**.
 34. Clinical and Laboratory Standards Institute. *Performance Standards for Antimicrobial Disk and Dilution Susceptibility Tests for Bacteria Isolated from Animals: Approved Standard*. Clinical and Laboratory Standards Institute: Wayne, USA, **2013**.
 35. Babahan, I.; Poyrazoglu-Coban, E.; Özmen, A.; Biyik, H. H.; Isman, B. Synthesis, Characterization and Biological Activity of Vic-Dioxime Derivatives Containing Benzaldehydehydrazone Groups and Their Metal Complexes. *Afr. J. Microbiol. Res.* **2011**, *5*, 271–283. DOI: [10.5897/AJMR10.622](https://doi.org/10.5897/AJMR10.622).
 36. Asegbeloyin, J. N.; Ujam, O. T.; Okafor, E. C.; Babahan, I.; Coban, E. P.; Ozmen, A.; Biyik, H. Synthesis, Characterization, and Biological Activity of N^o-(Z)-(3-Methyl-5-Oxo-1-Phenyl-1,5-Dihydro-4H-Pyrazol-4-Ylidene)(Phenyl)methylBenzohydrazide and Its Co(II), Ni(II), and Cu(II) Complexes. *Bioinorg. Chem. Appl.* **2014**, *2014*, 718175. DOI: [10.1155/2014/718175](https://doi.org/10.1155/2014/718175).
 37. Şahin, Y.; Çoban, E. P.; Sevinçek, R.; Biyik, H. H.; Özgür, H.; Aygün, M. 1,2-Diborolanes with Strong Donor Substituents: Synthesis and High Antimicrobial Activity. *Bioorg. Chem.* **2021**, *106*, 104494. DOI: [10.1016/j.bioorg.2020.104494](https://doi.org/10.1016/j.bioorg.2020.104494).
 38. Asegbeloyin, J. N.; Babahan, I.; Ukwueze, N. N.; Oruma, U. S.; Poyrazoglu, E.; Eze, U. F.; Biyik, H. H. Synthesis, Characterization and Antimicrobial Activity of 3-Acetyl-4-Hydroxy-6-Methyl-(2H) Pyran-2-One Schiff Base with 2, 2'-(Ethylenedioxy) Diethylamine and Its Co(II), Ni(II) and Cu(II) Complexes. *Asian J. Chem.* **2015**, *27*, 3345–3349. DOI: [10.14233/ajchem.2015.18712](https://doi.org/10.14233/ajchem.2015.18712).
 39. Babahan, I.; Özmen, A.; Aslan, K. Synthesis and Use of Dioxime Ligands for Treatment of Leukemia and Colon Cancer Cells. *Appl. Organometal. Chem.* **2017**, *31*, e3752. DOI: [10.1002/aoc.3752](https://doi.org/10.1002/aoc.3752).
 40. Babahan, I.; Özmen, A.; Aksel, M.; Bilgin, M. D.; Gumusada, R.; Gunay, M. E.; Eydurhan, F. A Novel Bidentate Ligand Containing Oxime, Hydrazone and Indole Moieties and Its BF₂⁺ Bridged Transition Metal Complexes and Their Efficiency against Prostate and Breast Cancer Cells. *Appl. Organomet. Chem.* **2020**, *34*, e5632. DOI: [10.1002/aoc.5632](https://doi.org/10.1002/aoc.5632).
 41. Frisch, M. J.; Trucks, G. W.; Schlegel, H. B.; Scuseria, G. E.; Robb, M. A.; Cheeseman, G.; Scalmani, J. R.; Barone, V.; Mennucci, V. *Gaussian 09, Revision A.02*. Gaussian, Inc., Wallingford, **2009**.
 42. Okagu, O. D.; Ugwu, K. C.; Ibeji, C. U.; Ekennia, A. C.; Okpareke, O. C.; Ezeorah, C. J.; Anarado, C. J.; Babahan, I.; Coban, B.; Yıldız, U.; et al. Synthesis and Characterization of Cu(II), Co(II) and Ni(II) Complexes of a Benzohydrazone Derivative: Spectroscopic, DFT, Antipathogenic and DNA Binding Studies. *J. Mol. Struct.* **2019**, *1183*, 107–117. DOI: [10.1016/j.molstruc.2019.01.069](https://doi.org/10.1016/j.molstruc.2019.01.069).
 43. Ekennia, A. C.; Ibezim, E. C.; Okpareke, O. C.; Ibeji, C. U.; Babahan, I.; Coban, B.; Abulhasanov, B.; Cömert, F.; Ujam, O. T. Novel 3-Hydroxy-2-Naphthoic Hydrazone and Ni(II), Co(II) and Cu(II) Complexes: Synthesis, Spectroscopic Characterization, Antimicrobial, DNA Cleavage and Computational Studies. *Appl. Organomet. Chem.* **2019**, *33*, 1–14. DOI: [10.1002/aoc.4913](https://doi.org/10.1002/aoc.4913).
 44. Kathawate, L.; Joshi, P. V.; Dash, T. K.; Pal, S.; Nikalje, M.; Weyhermüller, T.; Puranik, V. G.; Konkimalla, V. B.; Salunke-Gawali, S. Reaction between Lawsone and Aminophenol Derivatives: Synthesis, Characterization, Molecular Structures and Antiproliferative Activity. *J. Mol. Struct.* **2014**, *1075*, 397–405. DOI: [10.1016/j.molstruc.2014.07.007](https://doi.org/10.1016/j.molstruc.2014.07.007).
 45. Kalsi, P. S. *Spectroscopy of Organic Compounds*, 6th ed.; New Age Int Ltd Publishers: New Delhi, **2004**.
 46. Feizi, N.; Pinjari, R. V.; Gejji, S.; Sayyed, F.; Gonnade, R.; Rane, S. Y. Crystal Structure, NMR and Theoretical Investigations on 2-(o-Hydroxy-Anilino)-1,4-Naphthoquinone. *J. Mol. Struct.* **2010**, *966*, 144–151. DOI: [10.1016/j.molstruc.2009.12.029](https://doi.org/10.1016/j.molstruc.2009.12.029).
 47. Ekennia, A. C.; Osowole, A. A.; Onwudiwe, D. C.; Babahan, I.; Ibeji, C. U.; Okafor, S. N.; Ujam, O. T. Synthesis, Characterization, Molecular Docking, Biological Activity and Density Functional Theory Studies of Novel 1,4-Naphthoquinone Derivatives and Pd(II), Ni(II) and Co(II) Complexes. *Appl. Organometal. Chem.* **2018**, *32*, e4310. DOI: [10.1002/aoc.4310](https://doi.org/10.1002/aoc.4310).
 48. Osowole, A. A.; Ekennia, A. C.; Olubiyi, O. O.; Olagunju, M. Synthesis, Spectral, Thermal, Antibacterial and Molecular Docking Studies of Some Metal(II) Complexes of 2-(1,3-Benzothiazol-2-Ylamino)Naphthalene-1,4-Dione. *Res. Chem. Intermed.* **2017**, *43*, 2565–2585. DOI: [10.1007/s11164-016-2780-8](https://doi.org/10.1007/s11164-016-2780-8).
 49. Yang, T. L.; Qin, W. W. Transition Metal Manganese(II), Nickel(II), Copper(II) and Zinc(II) Complexes of a New Schiff Base Ligand: Synthesis, Characterization and Antitumor Activity Studies. *Pol. J. Chem.* **2006**, *80*, 1657.
 50. Kargar, H.; Fallah-Mehrjardi, M.; Behjatmanesh-Ardakani, R.; Rudbari, H. A.; Ardakani, A. A.; Sedighi-Khavidak, S.; Munawar, K. S.; Ashfaq, M.; Tahir, M. N. Binuclear Zn(II) Schiff Base Complexes: Synthesis, Spectral Characterization, Theoretical Studies and Antimicrobial Investigations. *Inorg. Chim. Acta.* **2022**, *530*, 120677. DOI: [10.1016/j.ica.2021.120677](https://doi.org/10.1016/j.ica.2021.120677).
 51. Kargar, H.; Fallah-Mehrjardi, M.; Behjatmanesh-Ardakani, R.; Amiri Rudbari, H.; Ardakani, A. A.; Sedighi-Khavidak, S.; Munawar, K. S.; Ashfaq, M.; Tahir, M. N. Synthesis, Spectral Characterization, Crystal Structures, Biological Activities, Theoretical Calculations and Substitution Effect of Salicylidene Ligand on the Nature of Mono and Dinuclear Zn(II) Schiff Base Complexes. *Polyhedron.* **2022**, *213*, 115636. DOI: [10.1016/j.poly.2021.115636](https://doi.org/10.1016/j.poly.2021.115636).
 52. Kargar, H.; Ardakani, A. A.; Tahir, M. N.; Ashfaq, M.; Munawar, K. S. Synthesis, Spectral Characterization, Crystal Structure Determination and Antimicrobial Activity of Ni(II), Cu(II) and Zn(II) Complexes with the Schiff Base Ligand Derived from 3,5-Dibromosalicylaldehyde. *J. Mol. Struct.* **2021**, *1229*, 129842. DOI: [10.1016/j.molstruc.2020.129842](https://doi.org/10.1016/j.molstruc.2020.129842).
 53. Hazhaz, H.; Melkemi, N.; Salah, T.; Bouachrine, M. DFT-Based Reactivity and Combined QSAR, Molecular Docking of 1,2,4,5-Tetrazine Derivatives as Inhibitors of Pim-1 Kinase. *Heliyon.* **2019**, *5*, e02451. DOI: [10.1016/j.heliyon.2019.e02451](https://doi.org/10.1016/j.heliyon.2019.e02451).